Politecnico di Torino

Corso di Laurea in

Mechanical Engineering

Tesi di laurea

Lock-in thermography for residual stresses investigation in steel welded joints

Relatori

Prof.ssa Raffaella Sesana

Prof.ssa Francesca Curà

Ing. Rosario Molica Nardo

Ing. Dario Rini

Ing. Luca Corsaro

Ing. Irene Pessolano Filos

Candidato

Luca Santoro

Dipartimento di Ingegneria Meccanica e Aerospaziale

DIMEAS

Anno Accademico 2020/2021

Abstract

A non-destructive method for the residual stresses evaluation in welded joints is here proposed. Conventional residual stress determination techniques are based on the destruction of the original material stress state that causes a relaxation, hence is not possible to use those methods on working components. The proposed method provides for an active lock-in infrared thermography analysis by means of a FLIR thermal camera and an exciting laser head for the evaluation of the thermal diffusivity. In general, it is possible to relate the thermal diffusivity to the diffusion length, which is the ability of a thermal wave with a known wavelength to penetrate inside the sample, using the phase contrast trend as a function of the distance from the laser spot. Through the variation in diffusivity is possible to investigate the level of anisotropy in the Heat Affected Zone (HAZ). On the basis of these considerations, tests were run by varying thermal source parameters, as laser power level and number of impulses in the time unit. The post-processing of the experimental data needs to face high noise to signal ratio and phase mapping extraction algorithm, therefore Single Value Decomposition (SVD)-denoising and lock-in amplifier techniques were implemented in a Matlab script. Thus, the diffusivity is expected to be dependent on the local characteristics in the joint and varying through the different directions Preliminary experimental results obtained on custom made welded joint samples are presented and discussed

Summary

Abstract 3

Introduction and principles 6

State of art 8

Residual Stresses investigation 8

Analytical model: Quantitative analysis of diffusivity 12

Thermally thin slab (l<<μ) 13

Thermally thick slab (l>> μ) 15

Comments 15

SVD-Denoising 16

Comments 30

Cattaneo-Vernotte Model for short impulse 31

Numerical Simulation of Cattaneo Vernotte model 35

Pulsed Calibration 38

Comments 39

Materials 40

Equipment 41

Assessing emissivity 42

Pulsed 43

Preliminary study 44

Pulsed Calibration 45

Results and discussion 50

Lock in 51

Introduction to Lock-in routine 51

Laser power\harmonics\methods comparisons 54

Base Metal vs Welded joint [With\Without residual stresses] 69

Comments 75

Metallographic analysis 77
Comments 77
Specimen 1 78
Base metal 78
HAZ 79
Weld bead 80
Specimen 2 81
Base metal 81
HAZ 82
Weld bead 83
Conclusions 84
References 86

Introduction and principles

This work born from the collaboration between **ADES Group** and **DiMeAs** department of **Politecnico di Torino**.

Active infra-red thermography (Active IRT) is becoming widely used as effective non destructive testing for defect investigation.

However the application of this technology for residual stresses on welded joint investigation has not been studied. In addition the the close dependence of the of the results by the environmental condition of the test and the surface thermal properties makes difficult the calibration of this model. So, a pure qualitative comparison between different specimens can't work and all the phenomena involved in the technique needs to be taken into account. Thus an accurate study of the state of art has been done to understand the feasibility of a new method for the detection and characterization of residual stresses presence and severity.

The active-IRT technique consists in recording and analysing the thermal response of a component subjected to an external heat excitation. The thermogram resulting from the test is the record of the infra-red spectrum of light which is calibrated by knowing ambient parameter and emissivity of the investigated specimen to pass from the wave's energy to a temperature value.[1]

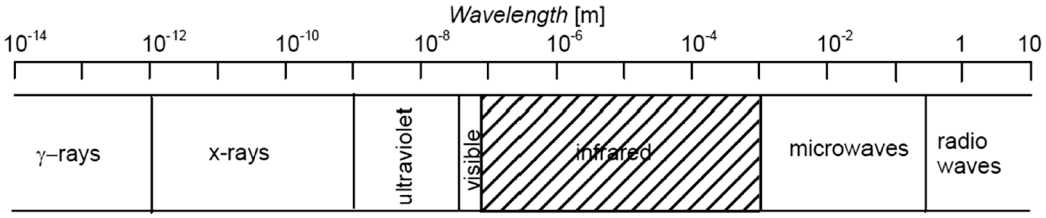

Then will follow some basics definitions that must be reminded before going through the problem

By the definition of black body, an ideal surface which only absorb energy, is possible to define the emissivity for the whole spectrum as:

$$E_b = \sigma * T^4$$

Where σ is the Stefan-Boltzmann constant and T the absolute temperature. The real component won't follow exactly this law because is capable to transmit and reflect radiative energy. This is valid for the test article, the ambient where the test is performed, the atmosphere.

So, the energy detected by the camera will be:

$$E_{TOT} = E_{obj} + E_{refl} + E_{atm}$$

Where E_{tot} is the total energy detected, E_{obj} is the energy emitted by the component being tested, E_{refl} is the energy reflected by the ambient, E_{atm} is the energy emitted by the atmosphere. In real component the phenomenon is dependent by the frequency range

Different material properties and geometries affects the the thermal diffusivity, this can be read as different thermal dynamic behaviour of the investigated zone. The main techniques work on this principle. By studying the thermogram resulting from a dynamic thermal excitation is possible detect flaws in the material, the most used technique are the pulsed and lock-in thermography.

The governing equation of the physic of the problem is the Fourier equation:

$$\frac{\delta T}{\delta t} = \alpha \frac{\delta^2 T}{\delta z^2}$$

Where:

- T is the temperature in [K]
- α is the thermal diffusivity [m^2 /s] defined as:

$$\alpha = \frac{k}{\rho c}$$

Where k is the thermal conductivity [W/(mK)], ρ the density [Kg/m^3] and c the specific heat[J/(KgK)]

State of art

Residual Stresses investigation

From [2] a investigation through laser beam lock-in thermography on residual stresses has been performed on plastically deformed specimen.

This work perform both a quantitative and qualitative analysis to show the effect of the anisotropy induced by plastic deformation of the steel on thermal properties. A similar approach will be used in this work.

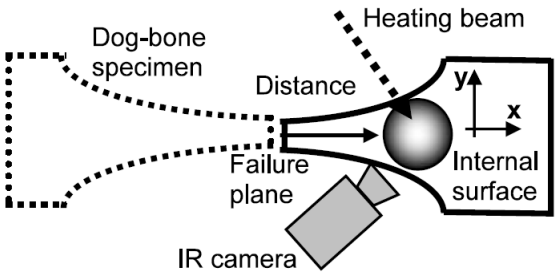

The specimen is excited locally using a laser beam, then the phase of the thermal response is used to characterize the thermal diffusivity, in the end a comparison is done between different areas of the specimen.

$$\Phi(r) = \Phi_o - \frac{r}{\mu}$$

Where:

- Φ Phase
- r distance from the laser spot
- μ thermal diffusion length defined as:

$$\mu = \sqrt{\frac{D}{\pi f}}$$

where:

- D thermal diffusivity
- f modulation frequency of the laser

So the thermal diffusion length take the meaning of the slope of the phase in relation to the distance from the laser spot

In the image is possible to see the phase map of the thermal response, the phase obtained in the plastically deformed zone shows clearly an anisotropy.

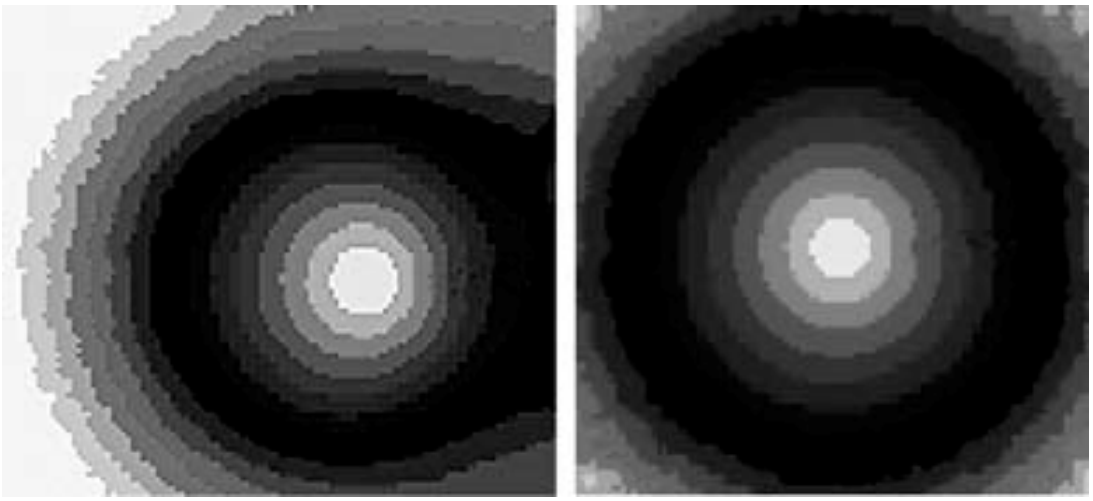

So the idea is to quantitatively characterize the anisotropy by means of the thermal diffusivity.

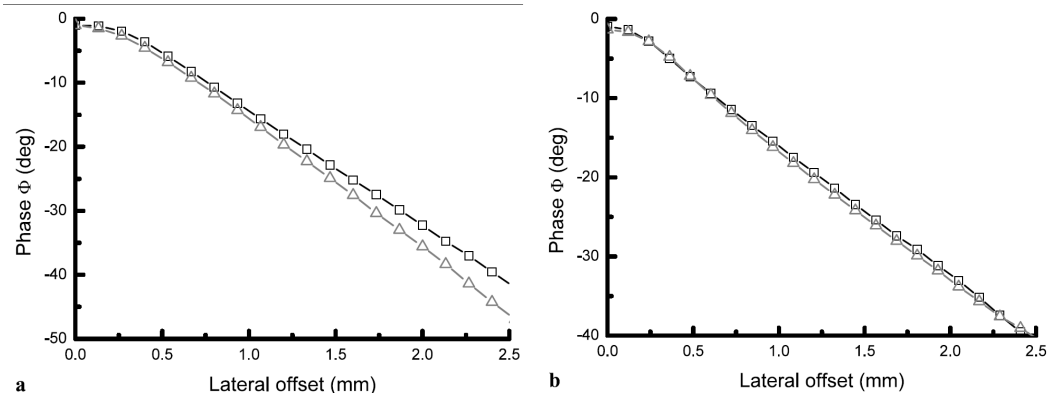

Then cutting the phase map through the two perpendicular axis x and y and confronting it can be seen that the phase has two different slope in the case of the test performed in the plastical deformed zone while the slope is the same in the isotropic zone.

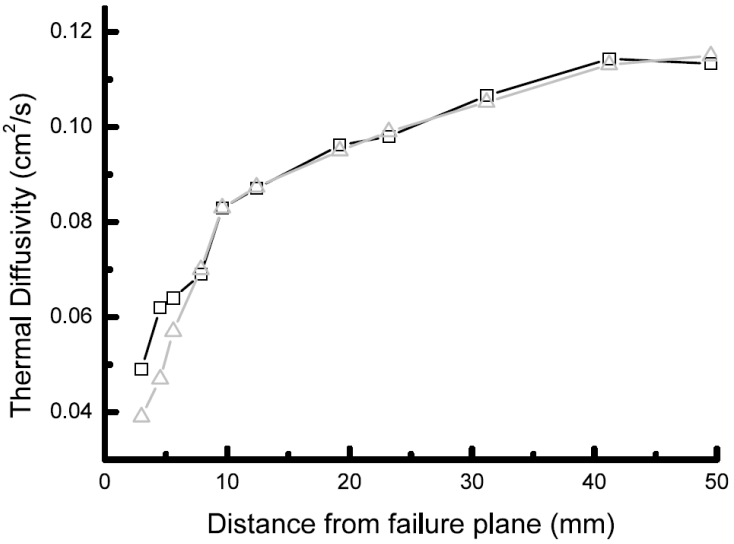

Thermal diffusivity as a function of the distance from the failure plane. The reported values have been respectively obtained considering the profiles parallel (squares) and orthogonal (triangles) to the direction x of the applied tensile load

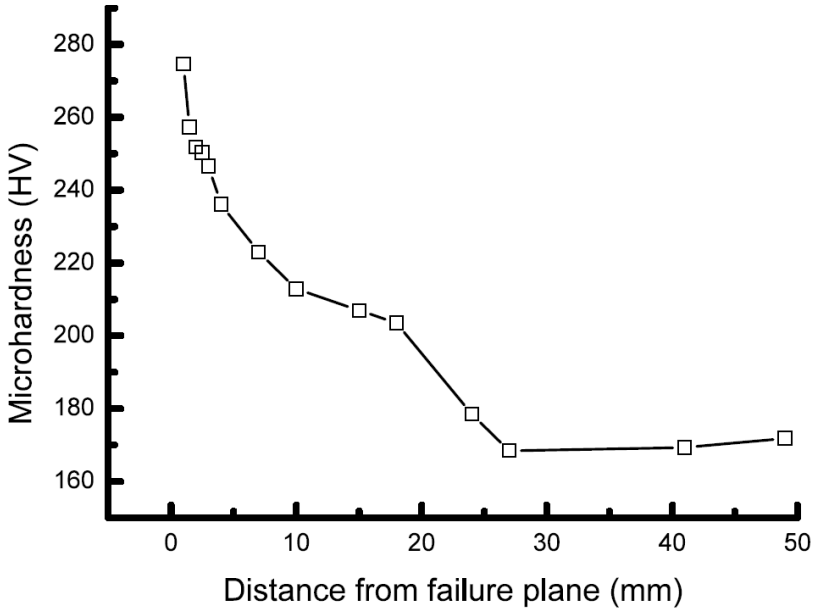

Therefore the plastic deformation induces a change in thermal diffusivity, this can be qualitatively related to microhardness and microstructure

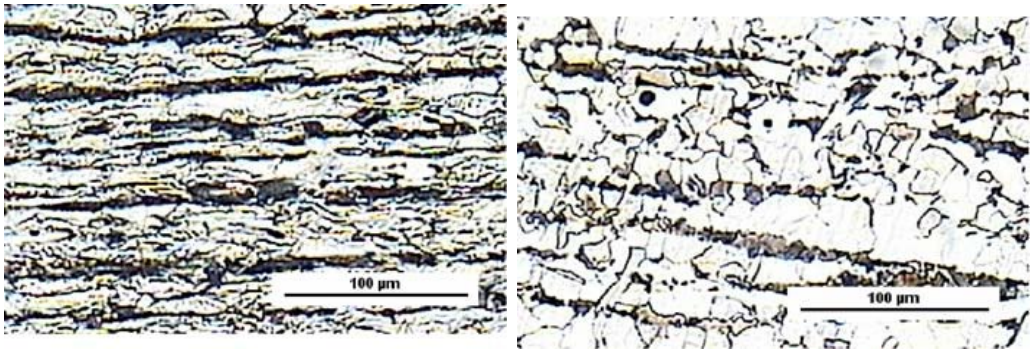

Micrographs respectively corresponding to the surface areas close to the failure plane (**left**) and 4 cm far from it (**right)**

Analytical model: Quantitative analysis of diffusivity

The work [3] investigates the effect of boundary condition to have good thermal diffusivity measurement of thin/thick plates, even in the case of anisotropy, using laser beam lock-in thermography.

While in some case we can say that there is a linear relation between the phase of the surface temperature and the lateral distance of the heating spot, such as in the case of stiff plates where we can neglect the heat losses, this is not always true. Starting from an analytical model is possible to asses the measurement in case of thin plates and filaments

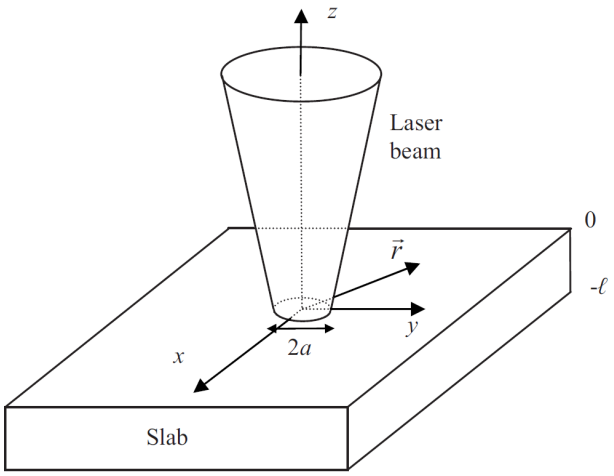

Here is reported the analytical study of [3]for an anisotropic slab.

Let us consider a slab of thickness l, heated by a laser beam of power P_0 with a gaussian profile of radius a(at $1/e^2$) and modulated at frequency f.

$$T_{ac}(x,y,z) = \int_{-\infty}^{\infty}\int_{-\infty}^{\infty} e^{-i(x\lambda+y\eta)}[A'e^{\gamma z} + B'e^{-\gamma z}]d\lambda d\eta$$

Where λ, η are the Fourier Variables and $\gamma^2 = \frac{D_x\lambda^2 + D_y\lambda^2 + i\omega}{D_z}$. A' and B' are constants to be determined from the heat flux continuity at the sample surface.

$$K_z \frac{\partial T_{ac}}{\partial z}\Big|_{z=0} + h_o T_{ac}|_{z=0} = \frac{P_0}{4\pi}\int_{-\infty}^{\infty}\int_{-\infty}^{\infty}\left(e^{-i(x\lambda+y\eta)}e^{-\frac{(\lambda^2+\eta^2)a^2}{8}}\right)d\lambda d\eta$$

$$K_z \frac{\partial T_{ac}}{\partial z}\Big|_{z=-l} - h_1 T_{ac}|_{z=-l} = 0$$

$$T_{ac}(x,y,z) = \frac{P_0}{4k\pi}\int_{-\infty}^{\infty}\int_{-\infty}^{\infty}\frac{e^{-i(x\lambda+y\eta)}e^{-\frac{(\lambda^2+\eta^2)a^2}{8}}}{\gamma}$$
$$\times\left[\frac{(1+H_1')e^{\gamma l}e^{\gamma z} + (1-H_1')e^{-\gamma l}e^{-\gamma z}}{(1+H_0')(1+H_1')e^{\gamma l} - (1-H_0')(1-H_1')e^{-\gamma l}}\right]d\lambda d\eta$$

Where $H'_0 = h_0/K_z\lambda$

Then are analysed two extreme cases of interest :

- Thermally thin slab
- Thermally thick slab

Thermally thin slab (l<<μ)

The equation reduces to

$$T_{ac}(x,y) = \frac{\frac{P_0}{4\pi\rho c l}\int_{-\infty}^{\infty}\int_{-\infty}^{\infty} e^{-i(x\lambda+y\eta)} \times e^{-\frac{(\lambda^2+\eta^2)a^2}{8}}}{D_x\lambda^2 + D_y\eta^2 + i\omega + \frac{2h}{\rho c l}}\, d\lambda d\eta$$

Where $\rho c = \frac{K_x}{D_x} = \frac{K_y}{D_y} = \frac{K_z}{D_z}$ is the heat capacity.

For a highly focused laser beam (a=0) the precedent equation has analytical solution along the principal axes

$$T_{ac}(x, a = 0) = \frac{P_0}{2\rho c l} \frac{1}{\sqrt{D_x D_y}} K_0(\sigma'_x x)$$

$$T_{ac}(y, a = 0) = \frac{P_0}{2\rho c l} \frac{1}{\sqrt{D_x D_y}} K_0(\sigma'_y y)$$

Where : $\sigma'^2_{x,y} = \frac{i\omega}{D_{x,y}} + \frac{2h}{K_{x,y} l}$

Using the asymptotic approach for large x and y values the equation reduces to

$$T_{ac}(x \to \infty, a = 0) \approx \frac{P_0}{2\rho c l} \frac{1}{\sqrt{D_x D_y}} \sqrt{\frac{\pi}{2\sigma'_x}} \frac{e^{-\sigma'_x x}}{\sqrt{x}}$$

$$= \frac{P_0}{2\rho c l} \frac{1}{\sqrt{D_x D_y}} \sqrt{\frac{\pi}{2}} \frac{1}{\sqrt{\sigma'_{xR} + i\sigma'_{xI}}} \frac{e^{-\sigma'_{xR} x}}{\sqrt{x}} e^{i\sigma'_{xI} x}$$

$$T_{ac}(y \to \infty, a = 0) \approx \frac{P_0}{2\rho c l} \frac{1}{\sqrt{D_x D_y}} \sqrt{\frac{\pi}{2\sigma'_y}} \frac{e^{-\sigma'_y y}}{\sqrt{y}}$$

$$= \frac{P_0}{2\rho c l} \frac{1}{\sqrt{D_x D_y}} \sqrt{\frac{\pi}{2}} \frac{1}{\sqrt{\sigma'_{yR} + i\sigma'_{yI}}} \frac{e^{-\sigma'_{yR} y}}{\sqrt{y}} e^{i\sigma'_{yI} y}$$

Where $\sigma'_{xR}, \sigma'_{xI}, \sigma'_{yR}, \sigma'_{yI}$ are the real and imaginary part of σ'_x, σ'_y.

The main result from this study is that the phase and the natural logarithm of the temperature amplitude multiplied by $\sqrt{x}\ or\ \sqrt{y}$ have a linear dependence on the distance from the laser spot such that the product of the slope is equal to $-\pi f/D_x$ and $-\pi f/D_y$.

The finite laser spot size $a \neq 0$ does not affect the slopes

Thermally thick slab (l>> μ)

In this case the surface temperature is given by

$$T_{ac}(x,y,z=0) = \frac{P_0}{4\pi K_z} \int_{-\infty}^{\infty} e^{-i(x\lambda+y\eta)} \ \frac{e^{-(\lambda^2+\eta^2)\frac{a^2}{8}}}{\lambda + \frac{h_0}{K_z}}\, d\lambda d\eta$$

By numerical simulation has been shown that, in the absence of heat loss, the natural logarithm of the temperature amplitude multiplied by x or y and the phase have linear dependence on the distance with the same slope $-\sqrt{\frac{\pi f}{D_x}}$, $-\sqrt{\frac{\pi f}{D_y}}$. Anyway heat losses are usually negligible.

Comments

In this work a complete investigation of boundary condition has been performed. One of the main remark to be consider is the effect of high temperature rise on linearity of the physic of the problem.

This is a big challenge because this leads to low signal to noise ratio so a stiff signal processing algorithm is needed , in fact is suggested to use a 2K maximum temperature increase over the environmental temperature.

Another two important suggestion come us by this work, the first is to use a black paint layer to asses reflection phenomena, but the thickness of the layer must be negligible with respect to the specimen one, the second is to avoid high frequency (>10Hz) to avoid diffraction interference.

Performing the tests in vacuum suppress convective heat losses, in particular in the case of low diffusivity material.

SVD-Denoising

The work [4] present a method for singular value decomposition denoising, the most significative parts will be reported here.

Starting from a theoretical prediction of the root mean square error of the SVD modes, which is defined as

$$rmse(\tilde{\mathrm{v}}_{\boldsymbol{k}}) \equiv \left[\frac{1}{D}\sum_{i=1}^{D}(\tilde{\mathrm{v}}_{ik} - v_{ik})^2\right]^{\frac{1}{2}}$$

The key idea of our proposed noise filtering method is to use only the modes for which the rmse is sufficiently below this noise ceiling. Herein, is proposed the following method for minimum loss noise filtering from[4].

1. Given a noisy data matrix $\tilde{A}$, perform the SVD (Matlab svd command) to obtain $\widetilde{\boldsymbol{u_k}}$ $\widetilde{s_k}$ $\widetilde{v_k}$

2. Estimate the measurement error $\bar{\epsilon}$ and the 'spatial correlation parameter' f by fitting a Marchenko–Pastur distribution to the tail of the noisy singular values.

3. (Optional) Infer the '*effective smoothing window width*',**w**, from the curve fit, which reads

$$w = 1 + \left(2f - \frac{3}{2}\right)\left(1 - e^{-20(f-1)}\right)$$

4. Estimate the root mean square error of the modes:

$$rmse(\tilde{\boldsymbol{v}}_k) \approx min\left\{\sqrt{2/D}\,, \frac{\bar{\varepsilon}}{\widetilde{S_k}}\left[\frac{D-w}{D} + \frac{w}{D}\sum_{\substack{m=1\\ m\neq k}}^{T}\frac{\tilde{\lambda}_{m(3\widetilde{\lambda_k}-\widetilde{\lambda_m})}}{(\tilde{\lambda}_m-\tilde{\lambda}_k)^2}\right]^{\frac{1}{2}}\right\}$$

Where $\widetilde{\lambda_k} \equiv \widetilde{s_k^2}$.

$\widetilde{s_k}$ ia the noisy mode k D are the data sites and T the timesteps

5. Estimate the rank for minimum-loss reconstruction as follows:

$$t_k \equiv \frac{log\big(rmse(\tilde{\mathbf{v}}_k)\big) - log\left(\sqrt{2/D}\right)}{log\big(rmse(\tilde{\mathbf{v}}_1)\big) - log\left(\sqrt{2/D}\right)}$$

$$\bar{r}_{min} \equiv \text{maximum k such that } t_k > 5\%$$

The parameter tk quantifies the cleanliness of a mode, where t1 = 1 for the first (cleanest) mode, and tk = 0 for modes at the noise ceiling (rmse(ṽ k) = √ 2/D) .Modes that are sufficiently below this noise ceiling (i.e. that have a large enough tk) are deemed clean enough to be useful for data reconstruction. The threshold in was set at 5% .

6. Reconstruct an estimate of the clean singular values:

$$\bar{S}_k = \begin{cases} \sqrt{\check{S}_k^2 - (\epsilon' \hat{s}_k)^2} & if\ (k < k_c) \\ 0 & if\ (k_c \leq k) \end{cases}$$

where$\epsilon' \hat{s}_k$ is a Marchenko–Pastur distribution, and kc is the minimum index k such $\widetilde{s_k} < \epsilon' \hat{s}_k$. This cutoff index ensures that yields a real number, and it sets $\widetilde{s_k}$ to zero for modes in the tail of the distribution, which are obliterated by noise Equation follows from the observation that

$$\tilde{S}_k^2 \approx S_k^2 + \left(\epsilon' \hat{S}_k\right)^2$$

7. Reconstruct an estimate of the clean data via

$$\bar{\mathbf{A}}_r = \sum_{k=1}^{r} \widetilde{\boldsymbol{u}}_k \bar{s}_k \widetilde{\boldsymbol{v}}_k^{\mathsf{T}}$$

with r = r̄min

Subsequently the method is improved by mean of singular modes.

For this part of the theory behind the denoising algorithm only the most important related to the work [5] parts will be discussed. In particular the part regarding the derivation of the approximation of the *root mean square error* and the *canonical angles* of the modes will not be presented.

Perturbation theory is used to derive expressions for the expected values and standard deviations of the noisy singular values and vectors

The *temporal autocorrelation matrix* $\boldsymbol{H} \in R^{T\times T}$ for the analytic data is defined as:

$$\mathbf{H} \equiv \mathbf{A}\mathbf{A}^{\intercal}$$

The temporal autocorrelation matrix $\mathbf{H}$ for the noisy data $\widetilde{\mathbf{A}} = \mathbf{A} + \mathbf{E}$ is thus defines as

$$\widetilde{\mathbf{H}} \equiv \widetilde{\mathbf{A}}\widetilde{\mathbf{A}}^{\intercal} = \mathbf{A}\mathbf{A}^{\intercal} + \mathbf{A}\mathbf{E}^{\intercal} + \mathbf{E}\mathbf{A}^{\intercal} + \mathbf{E}\mathbf{E}^{\intercal}, \equiv \mathbf{H} + \varepsilon\widehat{\mathbf{H}}^{(2)}$$

where $\widehat{\mathbf{H}}^{(1)} \equiv \mathbf{A}\widehat{\boldsymbol{E}}^{\intercal} + \hat{\mathbf{E}}\boldsymbol{A}^{\intercal}$ and $\widehat{\mathbf{H}}^{(2)} \equiv \hat{\mathbf{E}}\hat{\mathbf{E}}^{\intercal}$

Continuing with the required definitions, now define the projection matrix $\boldsymbol{P} \equiv \boldsymbol{A}\left(\boldsymbol{A}^{\boldsymbol{T}}\boldsymbol{A}\right)^{-\mathbf{1}} = \boldsymbol{U}\boldsymbol{U}^{\boldsymbol{T}}$, and define the mode k projection matrix by

$$\mathbf{P}_k \equiv \mathbf{u}_k\mathbf{u}_k^{\intercal}$$

Given vector **x** , the projection of **x** onto the column space of **A** is **Px-** , and the projection of **x** onto mode k is P_kx. Since$\boldsymbol{H}\boldsymbol{P}_{\boldsymbol{K}} = \lambda_k\boldsymbol{P}_{\boldsymbol{k}}$, it is natural to consider the reduced resolvent matrix

$$\mathbf{Q}_k \equiv \sum_{\substack{j=1 \\ j \neq k}}^{T} \frac{\mathbf{P}_j}{\lambda_j - \lambda_k}$$

Since$\boldsymbol{P_j P_k} = \boldsymbol{P_k}\delta_{jk}$, observe that$\boldsymbol{P_k Q_k} = \boldsymbol{Q_k P_k} = 0$, and thus

$$\mathbf{Q}_k^2 \equiv \sum j \neq k \frac{\mathbf{P}_j}{\left(\lambda_j - \lambda_k\right)^2}$$

We will define the ijth element of several matrices. Repeated indices other than i, j, or k indicate implied summation over 1,…, T or 1,…,D. Using index notation (but with no implied sum over k), we have

$$A_{ij} \equiv U_{im} S_{mn} V_{jn} = U_{im} V_{jm} s_m$$

$$H_{ij} \equiv A_{im} A_{jm} = U_{im} U_{jm} s_m^2$$

$$\widehat{H}_{ij}^{(1)} \equiv A_{im} \hat{E}_{jm} + \hat{E}_{im} A_{jm}$$

$$= \left(U_{in} \hat{E}_{jm} + \hat{E}_{im} U_{jn}\right) V_{mn} s_n$$

$$\widehat{H}_{ij}^{(2)} \equiv \hat{E}_{im} \hat{E}_{jm}$$

$$(\mathbf{P}_k)_{ij} \equiv U_{ik} U_{jk}$$

$$U_{mk} U_{mk} = 1$$

$$(\mathbf{Q}_k)_{ij} \equiv U_{im} U_{jm} (\lambda_m - \lambda_k)^{-1} (1 - \lambda_{mk})$$

In the case of spatially independent error data. Assuming each element of **E**, error matrix, is independent, identically distributed, all odd powers of **E** terms are expected to be zero for any combination of indices: ⟨Emn⟩ = 0 , ⟨EmnEpqErs⟩ = 0 , and so on. Some even power terms are as follows:

$$\langle E_{mn}E_{pq}\rangle = \epsilon^2\delta_{mp}\delta_{nq}$$

$$\langle E_{mn}E_{pn}\rangle = \epsilon^2 D\delta_{mp}$$

$$\langle E_{mn}E_{pq}E_{rs}E_{tu}\rangle = \epsilon^4\left[(\delta_{mp}\delta_{nq})(\delta_{rt}\delta_{su}) + (\delta_{mr}\delta_{ns})(\delta_{pt}\delta_{qu}) + (\delta_{mt}\delta_{nu})(\delta_{pr}\delta_{qs})\right]$$

Error data with spatial correlation can be modeled as that produced by uniform smoothing of i.i.d. random data as follows:

$$\boldsymbol{E}_{mn} = \frac{1}{w}\sum_{q=1}^{w}\bar{E}_{m,q-1+n-{}^{(w-1)}/_{2}}$$

For proof, consider ⟨E2mn⟩ , with no implied sum over m or n. Note that for the original i.i.d. data, ⟨Ɛ mnƐ pq⟩ =ϵ̄ 2 *δ* mp *δ*nq , so

$$\epsilon^2 = \langle E_{mn}^2\rangle = \langle\left(\frac{1}{w}\sum_{n=1}^{w}\bar{E}_{mn}\right)\left(\frac{1}{w}\sum_{q=1}^{w}\bar{E}_{mq}\right)\rangle = \frac{1}{w^2}\sum_{n=1}^{w}\sum_{q=1}^{w}\left(\bar{\epsilon}^2\delta_{nq}\right) = \frac{w\bar{\epsilon}^2}{w^2} = \frac{\bar{\epsilon}^2}{w}$$

Now consider the expected values of other useful **E** terms. The odd powers are still expected to be zero: ⟨Emn⟩ = 0 , ⟨EmnEpqErs⟩ = 0 , and so on. For perturbation theory, we are interested in sums across entire rows, such as $\sum_{q=1}^{D}\langle E_{mn}\bar{E}_{pq}\rangle$ This terms are evaluated as follows:

$$\langle E_{mn}E_{p,n+1}\rangle = \langle\left(\frac{1}{w}\sum_{n=1}^{w}\bar{E}_{mn}\right)\left(\frac{1}{w}\sum_{q=2}^{w+1}\bar{E}_{pq}\right)\rangle = \frac{1}{w^2}\sum_{n=1}^{w}\sum_{q=2}^{w+1}\left(\bar{\epsilon}^2\delta_{mp}\delta_{nq}\right) = \frac{w-1}{w}\epsilon^2\delta_{mp}$$

$$\langle E_{mn}E_{p,n+2}\rangle = \frac{1}{w^2}\sum_{n=1}^{w}\sum_{q=3}^{w+2}\left(\bar{\epsilon}^2\delta_{mp}\delta_{nq}\right) = \frac{w-2}{w}\epsilon^2\delta_{mp}$$

Thus, the desired cross-sum can be computed as follows:

$$\sum_{q=1}^{D}\langle E_{mn}E_{pq}\rangle = \left(\frac{1}{w}+\frac{2}{w}+\cdots+\frac{w-1}{w}+1+\frac{w-1}{w}+\cdots+\frac{1}{w}\right)\epsilon^2\delta_{mp} = w\epsilon^2\delta_{mp}$$

To make the perturbation theory analysis tractable the following "lumping" approximation is made:

$$\langle E_{mn}E_{pq}\rangle = w\epsilon^2\delta_{mp}\delta_{nq}$$

The approximation in last equation is to set all the q ≠ n terms in sum of errors on D to zero and instead to lump the contributions of these terms into the q = n term. The consequence of this lumping approximation is that in the perturbation theory analysis, various Apq terms are then only evaluated at q = n ; in other words, Apq takes the value Apn over the entire smoothing window. Since Apq is expected to vary only slightly over the smoothing window, this approximation is justified With the lumping approximation, the even power terms are now given as follows:

$$\langle E_{mn}E_{pq}\rangle = w\epsilon^2\delta_{mp}\delta_{nq}$$

$$\langle E_{mn}E_{pn}\rangle = \epsilon^2 D\delta_{mp}$$

$$\langle \| E \|_F\rangle = \langle\sqrt{E_{mn}E_{mn}}\rangle = \epsilon\sqrt{TD}$$

$$\langle E_{mn}E_{pq}E_{rs}E_{tu}\rangle = \epsilon^4 w^2\left[\left(\delta_{mp}\delta_{nq}\right)\left(\delta_{rt}\delta_{su}\right) + \left(\delta_{mr}\delta_{ns}\right)\left(\delta_{pt}\delta_{qu}\right) + \left(\delta_{mt}\delta_{nu}\right)\left(\delta_{pr}\delta_{qs}\right)\right]$$

Note a sum is implied across q = 1,…,D , and this cross-sum leads to the appearance of w,. In the last equation, cross-sums are implied across each {q, s, u} , which leads to the appearance of $\mathbf{w^2}$. By contrast, the weight w does not appear in others eq. , because the second index (n) is the same for both terms, and so no cross sum is implied (but rather just a regular sum over all n). Consider now other terms that appear in the perturbation theory derivations. Since all odd powers of **E** terms are expected to be zero, so to are odd "powers" of **H**(n) terms. That is, ⟨H(1) mn⟩ = ⟨H(1) mnH(2) pq ⟩ = ⟨H(1)mnH(1) pq H(1) rs ⟩ = ⋯ = 0 .

Some even "power" terms are these:

$$\begin{aligned}\langle H^{(1)}_{mn}H^{(1)}_{pq}\rangle &= \langle (A_{md}E_{nd} + E_{md}A_{nd})\big(A_{pe}E_{qe} + E_{pe}A_{qe}\big)\rangle \\ &= \langle A_{md}A_{pe}E_{nd}E_{qe} + A_{md}A_{qe}E_{nd}E_{pe} \\ &+ A_{nd}A_{pe}E_{md}E_{qe} + A_{nd}A_{qe}E_{md}E_{pe}\rangle \\ &= w\epsilon^2\big(H_{mp}\delta_{nq} + H_{mq}\delta_{np} + H_{np}\delta_{mq} + H_{nq}\delta_{mp}\big)\end{aligned}$$

(since only the e=d term survived)

$$\langle H^{(2)}_{mn}\rangle = \langle E_{md}E_{nd}\rangle = \epsilon^2 D\delta_{mn}$$

(since implied sum over d=1, …..,D)

$$\langle H^{(2)}_{mn}H^{(2)}_{pq}\rangle = \langle E_{md}E_{nd}E_{pe}E_{qe}\rangle = \epsilon^4 D^2\delta_{mn}\delta_{pq} + w^2\epsilon^4 D\big(\delta_{mp}\delta_{nq} + \delta_{mq}\delta_{np}\big)$$

$$\langle H^{(1)}_{mn}H^{(1)}_{pq}H^{(2)}_{rs}\rangle = \langle (A_{md}E_{nd} + E_{md}A_{nd})\big(A_{pe}E_{qe} + E_{pe}A_{qe}\big)\big(E_{rg}E_{sg}\big)\rangle$$
$$= \langle A_{md}A_{pe}E_{nd}E_{qe}E_{rg}E_{sg} + A_{md}A_{qe}E_{nd}E_{pe}E_{rg}E_{sg}$$
$$+ A_{nd}A_{pe}E_{md}E_{qe}E_{rg}E_{sg} + A_{nd}A_{qe}E_{md}E_{pe}E_{rg}E_{sg} +\rangle$$
$$= \epsilon^4\big[H_{mp}\big(wD\delta_{nq}\delta_{rs} + w^2\delta_{nr}\delta_{qs} + w^2\delta_{ns}\delta_{qr}\big)$$
$$+ H_{mq}\big(wD\delta_{np}\delta_{rs} + w^2\delta_{nr}\delta_{ps} + w^2\delta_{ns}\delta_{pr}\big)$$
$$+ H_{np}\big(wD\delta_{mq}\delta_{rs} + w^2\delta_{mr}\delta_{qs} + w^2\delta_{ms}\delta_{qr}\big)$$
$$+ H_{nq}\big(wD\delta_{mp}\delta_{rs} + w^2\delta_{mr}\delta_{ps} + w^2\delta_{ms}\delta_{pr}\big)\big]$$

The trace operation is $tr\,(\mathbf{X}) \equiv X_{mm}$, with implied sum over m=1,…..,*T.* Also note the identities $tr(\mathbf{X}+\mathbf{Y}) = tr(\mathbf{X}) + tr(\mathbf{Y})\ and\ \langle tr(\mathbf{X})\rangle = \langle tr(\mathbf{X})\rangle$. Thus

$$\langle tr\big(\widehat{\mathbf{H}}^{\mathbf{2}}\big)\rangle = \langle \hat{E}_{mn}\,\hat{E}_{mn}\rangle = TD,$$

$$tr\,\big(\widehat{\mathbf{H}}^2\mathbf{P}_k\big) = \langle \hat{E}_{mn}\,\hat{E}_{pn}\,U_{pk}\,U_{mk}\rangle = D\delta_{mp}\,U_{pk}U_{mk} = D,$$

$$\hat{\lambda}^{(1)}_k = tr\big[\mathbf{H}^{(1)}\mathbf{P}_k\big] = \big[\big(U_{pn}\hat{E}_{qm} + \hat{E}_{pm}U_{qn}\big)V_{mn}s_n\big]\big[U_{qk}U_{pk}\big] = 2s_kU_{qk}\hat{E}_{qm}V_{mk}\ ,$$

$$\langle\hat{\lambda}^{(1)}_k\rangle = 0$$

$$\langle\hat{\lambda}^{(2)}_k\rangle = \langle tr\big[\widehat{\mathbf{H}}^{(2)}\mathbf{P}_k - \big(\widehat{\mathbf{H}}^{(1)}\mathbf{Q}_k\big)\big(\widehat{\mathbf{H}}^{(1)}\mathbf{P}_k\big)\big]\rangle = D - \langle\hat{H}^{(1)}_{mn}(\mathbf{Q}_k)_{np}\hat{H}^{(1)}_{pq}(\mathbf{P}_k)_{qm}\rangle = D -$$
$$w\big(H_{mp}\delta_{nq} + H_{mq}\delta_{np} + H_{np}\delta_{mq} + H_{np}\delta_{mp}\big)\Big(U_{nl}U_{pl}(\lambda_l - \lambda_k)^{-1}(1 -$$
$$\delta_{lk})\Big)\big(U_{qk}U_{mk}\big) = D - w(\lambda_l + \lambda_k)(\lambda_l - \lambda_k)^{-1}(1 - \delta_{lk})\ .$$

$$\langle\Big(\hat{\lambda}^{(1)}_k\Big)^2\rangle = 4ws_k^2 = 4w\lambda_k$$

The final results are as follows:

$$\langle\left(W_{im}^{(1)}U_{mk}\right)^2\rangle = w\frac{\lambda_m+\lambda_k}{(\lambda_m-\lambda_k)^2}U_{im}^2(1-\delta_{mk})$$

$$\langle W_{im}^{(2)}U_{mk}\rangle = -\frac{w}{2}\frac{\lambda_m+\lambda_k}{(\lambda_m-\lambda_k)^2}(1-\delta_{mk})U_{ik}$$

$$\langle\left(N_{im}^{(1)}V_{mk}\right)^2\rangle = \frac{1-wV_{ik}^2}{\lambda_k} + w\frac{\lambda_m(3\lambda_k-\lambda_m)}{\lambda_k(\lambda_m-\lambda_k)^2}V_{im}^2(1-\delta_{mk})$$

$$\langle N_{im}^{(2)}V_{mk}\rangle = -\frac{1}{2\lambda_k}\left[D-w-w\frac{\lambda_m(3\lambda_k-\lambda_m)}{(\lambda_m-\lambda_k)^2}(1-\delta_{mk})\right]V_{ik}\ ,$$

with $(1-\delta_{mk})$ indicating a sum over m=1, ….,T but $m \neq k$.

Recall that the lumping approximation was used in precedent formulae ;so these formulae are also valid for the case of i.i.d. error data upon setting w = 1.

Both for completeness and because the singular values are the square roots of the eigenvalues $\widetilde{s_k} = \sqrt{\widetilde{\lambda_k}}$, we first consider the perturbed eigenvalues $\widetilde{\lambda_k}$. The kth eigenvalue of **H** can be written as a perturbation expansion

$$\tilde{\lambda}_k = \lambda_k + \epsilon\hat{\lambda}_k^{(1)} + \epsilon^2\hat{\lambda}_k^{(2)} + \cdots$$

where, assuming the eigenvalues of **H** are unique

$$\hat{\lambda}_k^{(1)} = tr\left[\widehat{\mathbf{H}}^{(1)}\mathbf{P}_k\right]$$

$$\hat{\lambda}_k^{(2)} = tr\left[\widehat{\mathbf{H}}^{(2)}\mathbf{P}_k - \left(\widehat{\mathbf{H}}^{(1)}\mathbf{Q}_k\right)\left(\widehat{\mathbf{H}}^{(1)}\mathbf{P}_k\right)\right]$$

Note that subscript k refers to the mode number, and no summation over k is implied. The expected value and standard deviation of $\widetilde{\lambda_k}$ are

$$\langle\tilde{\lambda}_k\rangle = \lambda_k + \epsilon^2\,\langle\hat{\lambda}_k^{(2)}\rangle + O(\epsilon^4)$$

$$\sigma_{\tilde{\lambda}_k} \equiv \sqrt{\langle\left(\tilde{\lambda}_k - \langle\tilde{\lambda}_k\rangle\right)^2\rangle} = \epsilon\sqrt{\langle\left(\hat{\lambda}_k^{(1)}\right)^2\rangle} + O(\epsilon^2)$$

Assuming that unique eigenvalues, and we extend his results to the case of spatially correlated error. We find

$$\langle\tilde{\lambda}_k = \lambda_k + \epsilon^2\left(D - w\sum_{\substack{m=1\\ m\neq k}}^{T}\frac{\lambda_m + \lambda_k}{\lambda_m - \lambda_k}\right) + O(\epsilon^4)\rangle$$

$$\sigma_{\tilde{\lambda}_k} = 2s_k\epsilon\sqrt{w} + O(\epsilon^2)$$

We now use the above results to find the perturbed singular values. Since the singular values of **A** are the square roots of the eigenvalues of **H** , we have

$$\tilde{s}_k = \sqrt{\tilde{\lambda}_k} = \sqrt{\lambda_k + \epsilon\hat{\lambda}_k^{(1)} + \epsilon^2\hat{\lambda}_k^{(1)} + \cdots}$$

If the error is small, then can be expanded in a Taylor series about λ_k,

$$\tilde{s}_k = \lambda_k^{\frac{1}{2}} + \frac{1}{2}\frac{1}{\lambda_k^{\frac{1}{2}}}\left(\epsilon\hat{\lambda}_k^{(1)} + \epsilon^2\hat{\lambda}_k^{(2)} + \cdots\right) - \frac{1}{2!}\frac{1}{4}\frac{1}{\lambda_k^{\frac{3}{2}}}\left(\epsilon\hat{\lambda}_k^{(1)} + \epsilon^2\hat{\lambda}_k^{(2)} + \cdots\right)^2 + \cdots$$

and upon substituting sk = √ λ_k , we have

$$\tilde{S}_k = S_k + \epsilon\left(\frac{\hat{\lambda}_k^{(1)}}{2_{s_k}}\right) + \epsilon^2\left(\frac{\hat{\lambda}_k^{(2)}}{2_{s_k}} - \frac{\left(\hat{\lambda}_k^{(1)}\right)^2}{8s_k^3}\right) + O(\epsilon^3)$$

The expected value and standard deviation of $\tilde{s}_k$ are

$$\langle\tilde{S}_k\rangle = S_k + \epsilon^2\left(\frac{\langle\hat{\lambda}_k^{(2)}\rangle}{2s_k} - \frac{\langle\left(\hat{\lambda}_k^{(1)}\right)^2\rangle}{8s_k^3}\right) + O(\epsilon^4)$$

$$\sigma_{\tilde{s}_k} \equiv \sqrt{\langle(\tilde{s}_k - \langle\tilde{s}_k\rangle)^2\rangle} = \epsilon\sqrt{\langle\left(\frac{\hat{\lambda}_k^{(1)}}{2s_k}\right)^2\rangle} + O(\epsilon^2)$$

$$\langle\tilde{S}_k\rangle = S_k + \frac{\epsilon^2}{2s_k}\left(D - w - w\sum_{\substack{m=1\\m\neq k}}^{T}\frac{\lambda_m + \lambda_k}{\lambda_m - \lambda_k}\right) + O(\epsilon^4)$$

$$\sigma_{\tilde{s}_k} = \epsilon\sqrt{w} + O(\epsilon^2)$$

Note that to first order, $\sigma_{\tilde{\lambda}_k} = 2s_k\sigma_{\tilde{s}_k}$, which makes sense since $\lambda_k = s_k^2$, so $d\lambda = 2s_k ds_k$

The kth left singular vector of **A**

$$\tilde{\mathbf{u}}_k = \mathbf{u}_k + c\mathbf{W}^{(1)}\mathbf{u}_k + c^2\mathbf{W}^{(2)}\mathbf{u}_k + \cdots$$

$$\tilde{U}_{ik} = U_{ik} + \epsilon W_{im}^{(1)}U_{mk} + \epsilon^2 W_{im}^{(2)}U_{mk} + \cdots$$

with implied summation over m=1,……,T, where

$$\mathbf{W}^{(1)} = \mathbf{Q}_k \widehat{\mathbf{H}}^{(1)} \mathbf{P}_k$$

$$\mathbf{W}^{(2)} = -\mathbf{Q}_k \widehat{\mathbf{H}}^{(2)} \mathbf{P}_k + \left(\mathbf{Q}_k \widehat{\mathbf{H}}^{(1)}\right)^2 \mathbf{P}_k - \mathbf{Q}_k^2 \left(\widehat{\mathbf{H}}^{(1)} \mathbf{P}_k\right)^2 - \frac{1}{2} \mathbf{P}_k \widehat{\mathbf{H}}^{(1)} \mathbf{Q}_k^2 \widehat{\mathbf{H}}^{(1)} \mathbf{P}_k$$

The expected value and standard deviation of $\widetilde{U}_{ik}$ are :

$$\langle \widetilde{U}_{ik} \rangle = U_{ik} + \epsilon^2 \langle W_{im}^{(2)} U_{mk} \rangle + O(\epsilon^4)$$

$$\sigma_{\widetilde{U}_{ik}} \equiv \left[\langle \left(\widetilde{U}_{ik} - \langle \widetilde{U}_{ik} \rangle \right)^2 \rangle \right]^{\frac{1}{2}} = \epsilon \left[\langle \left(W_{im}^{(1)} U_{mk} \right)^2 \rangle \right]^{\frac{1}{2}} + O(\epsilon^2)$$

Extending Venturi's results, with some effort to evaluate $\langle \left(W_{im}^{(1)} U_{mk} \right)^2 \rangle$ and $\langle W_{im}^{(2)} U_{mk} \rangle$ we find:

$$\langle \widetilde{U}_{ik} \rangle = \left(1 - \epsilon^2 \frac{w}{2} \sum_{\substack{m=1 \\ m \neq k}}^{T} \frac{\lambda_m + \lambda_k}{(\lambda_m - \lambda_k)^2} \right) U_{ik} + O(\epsilon^4)$$

$$\sigma_{\widetilde{U}_{ik}} = \epsilon \sqrt{w} \left[\sum_{\substack{m=1 \\ m \neq k}}^{T} \frac{\lambda_m + \lambda_k}{(\lambda_m - \lambda_k)^2} U_{im}^2 \right]^{\frac{1}{2}} + O(\epsilon^2)$$

The perturbed right singular vectors are evaluated.

The *k*th *right singular vector* of $\widetilde{\mathbf{A}}$ is:

$$\tilde{\mathbf{v}}_k = \mathbf{v}_k + \epsilon \mathbf{N}^{(1)}\mathbf{v}_k + \epsilon^2 \mathbf{N}^{(2)}\mathbf{v}_k + \cdots$$

$$\tilde{\mathrm{v}}_{ik} = \mathrm{v}_{ik} + \epsilon N_{im}^{(1)}\mathrm{v}_{mk} + \epsilon^2 N_{im}^{(2)}\mathrm{v}_{mk} + \cdots$$

With implied summation over m=1, ….. , D. gives $\mathrm{N}^{(2)}$

$$\mathbf{N}^{(1)} = \frac{1}{\lambda_k}\left(\mathbf{A}^{\intercal}\mathbf{W}^{(1)}\mathbf{A} + \widehat{\boldsymbol{E}}^{\intercal}\mathbf{A}\right) + \left(-\frac{1}{2}\frac{\hat{\lambda}_k^{(1)}}{\lambda_k}\right)\mathbf{I}$$

$$\mathbf{N}^{(2)} = \frac{1}{\lambda_k}\left(\mathbf{A}^{\intercal}\mathbf{W}^{(2)}\mathbf{A} + \widehat{\boldsymbol{E}}^{\intercal}\mathbf{W}^{(1)}\mathbf{A}\right) + \left(-\frac{1}{2}\frac{\hat{\lambda}_k^{(1)}}{\lambda_k^2}\right)\left(\mathbf{A}^{\intercal}\mathbf{W}^{(1)}\mathbf{A} + \widehat{\boldsymbol{E}}^{\intercal}\mathbf{A}\right) + \left(-\frac{1}{2}\frac{\hat{\lambda}_k^{(2)}}{\lambda_k} + \frac{3}{8}\frac{\left(\hat{\lambda}_k^{(1)}\right)^2}{\lambda_k^2}\right)\mathbf{I}$$

The expected value and standard deviation of $\tilde{V}_{ik}$ are

$$\langle \tilde{V}_{ik} \rangle = V_{ik} + \epsilon^2 \langle N_{im}^{(2)} V_{mk} \rangle + \mathrm{O}(\epsilon^4)$$

$$\sigma_{\tilde{v}_{ik}} \equiv \left[\langle \left(\tilde{V}_{ik} - \langle \tilde{V}_{ik} \rangle\right)^2 \rangle\right]^{\frac{1}{2}} = \epsilon \left[\langle \left(N_{im}^{(1)} V_{mk}\right)^2 \rangle\right]^{\frac{1}{2}} + \mathrm{O}(\mathrm{O}^2)$$

Extending Venturi's results, with some effort to evaluate $\langle \left(N_{im}^{(1)} V_{mk}\right)^2 \rangle$ and $\langle N_{im}^{(2)} V_{mk} \rangle$, we find

$$\langle \tilde{V}_{ik} \rangle = \left(1 - \frac{\epsilon^2}{\lambda_k} \left[\frac{D-w}{2} + \frac{w}{2} \sum_{\substack{m=1 \\ m \neq k}}^{T} \frac{\lambda_m (3\lambda_k - \lambda_m)}{(\lambda_m - \lambda_k)^2} \right] \right) V_{ik}$$

$$\sigma_{\tilde{V}_{ik}} = \frac{\epsilon}{s_k} \left[1 - w V_{ik}^2 + w \sum_{\substack{m=1 \\ m \neq k}}^{T} \frac{\lambda_m (3\lambda_k - \lambda_m)}{(\lambda_m - \lambda_k)^2} V_{im}^2 \right]^{\frac{1}{2}}$$

with $O(\epsilon^4)$ and $O(\epsilon^2)$ accuracy respectively

Furthermore more practical example are present in[4]–[6]

Comments

The application of this denoising algorithm lower the noise by approximately one order of magnitude, the purpose of this work is not to study the error produced by this method on different configuration while is to investigate the feasibility of the application on active thermography signal processing. In fact this method is commonly used in particle image velocimetry (PIV) but no application has been found on thermography.

In the image is shown the application on a pulsed thermography test, furthermore this is also applied in lock-in test which actually suffer of high noise ratio level in the boundaries of the laser beam thermally affected zone. This kind of processing improves the size of the zone where to apply the phase method without having noise problems and also permits to use lower temperature amplitude test's setup.

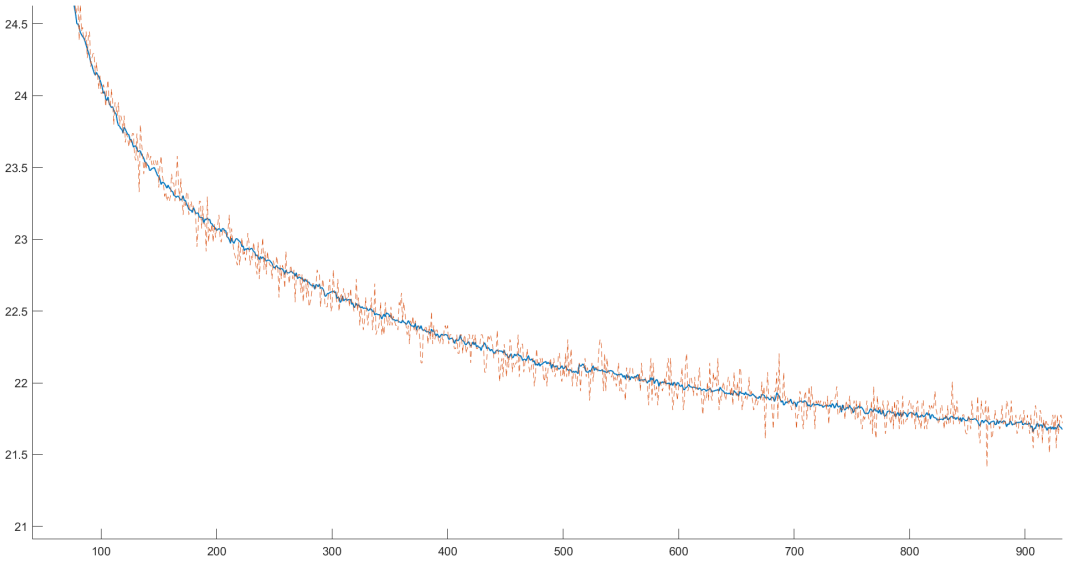

Cattaneo-Vernotte Model for short impulse

The governing equation of the physic of the problem is the Fourier equation:

$$\frac{\delta T}{\delta t} = \alpha \frac{\delta^2 T}{\delta z^2}$$

This is also called Diffusion Theory, it works for the most of the application and is easy to use. Anyway an approximation is done, the heat diffusion speed is consider inifinte.

A more accurate model is the Cattaneo Vernotte model[7], which is strictly related to the shock wave theory. Here we consider a finite heat diffusion speed C. In the case of an heat source moving with speed v, we are able to define the Mach number as:

$$Ma=v/C$$

This number characterize the thermal field nearby the heat source

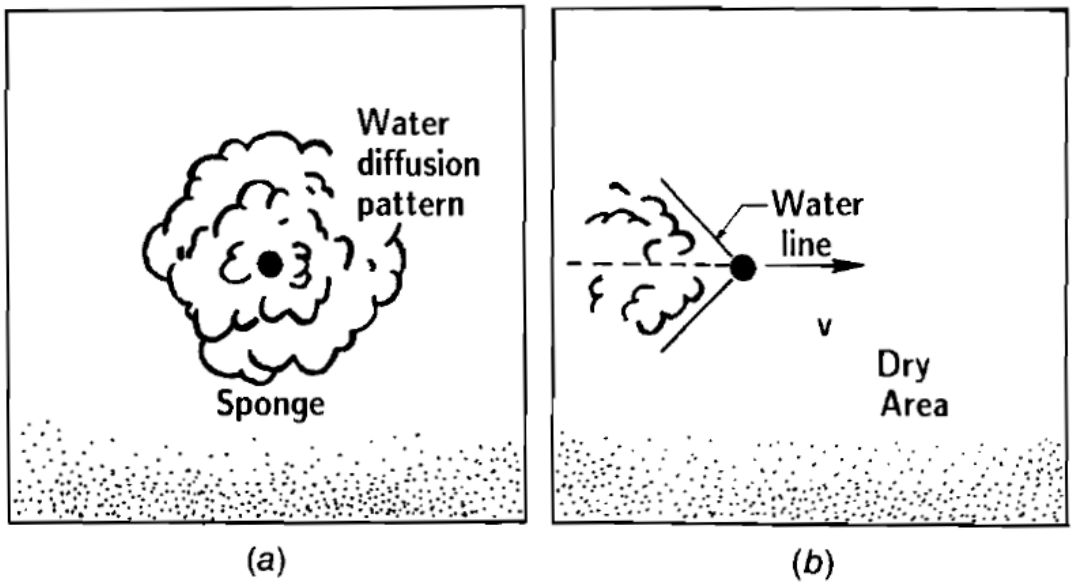

So the diffusion field will be divided into 2 zones: heat affected zone and unaffected zone.

If Ma>1 the source will create a shock wave. We are interested in the case (a) where the source is not moving.

The constitutive equation are

$$-\nabla * q + S = \rho C_p T_{,t}$$

$$\left(\frac{\alpha}{C^2}\right) q_{,t} + q = -k\nabla T$$

Where

- ρ=density
- C_p=heat capacity
- S=volumetric heat source
- C=heat diffusion speed

The we can define

α/C^2 =relaxation time

Notice:

If C goes to infinite we obtain the Fourier equation.

The diffusion model so can be expressed as depend on q or on T:

$$\nabla[\nabla * q] - \nabla S = \left(\frac{1}{\alpha}\right)\left[\left(\frac{\alpha}{C^2}\right) q_{,tt} + q_{,t}\right]$$

$$\alpha\nabla^2 T + \left(\frac{1}{\rho C_p}\right)\left[S + \left(\frac{\alpha}{C^2}\right) S_{,t}\right] = \left(\frac{\alpha}{C^2}\right) T_{,tt} + T_{,t}$$

The formation of the wavefront is expressed by defining a point source as a dirac delta

$$S(x_1, x_2, t) = Q\delta(x_1 + vt)\delta(x_2)$$

Then I substitute S(x1,x2,t) in the precedent equation

$$\alpha\nabla^2 T - \left(\frac{\alpha}{C^2}\right) T_{,tt} - T_{,t} = -\left(\frac{Q}{\rho C_p}\right)\left[\delta(x_1 - vt) + \left(\frac{\alpha}{C^2}\right)\delta_{,t}(x_1 - vt)\right]\delta(x_2)$$

And by means of Galilean transform

$$x_1 = \xi_1 + vt \text{ and } x_2 = \xi_2$$

I obtain

$$\alpha[(1 - M^2)T_{,11} + T_{,22}] + 2c\alpha T_{,1} = -\left(\frac{Q}{\rho C_p}\right)\left[\delta(\xi_1) - \left({}^{M^2}/_{2c}\right)\delta_{,1}(\xi_1)\right]\delta(\xi_2)$$

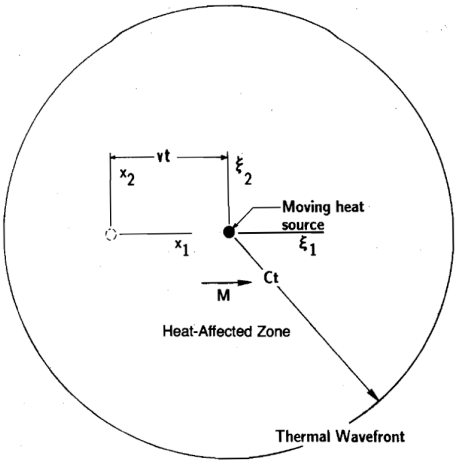

Figure 2 Thermal waves emanating from a moving heat source and the coordinate systems.

In the case of Mac<1 the solution of the differential equation is

$$\frac{T(\xi_i)}{{Q}/{\rho\alpha C_p}} = exp\left(-\frac{c\xi_1}{1 - M^2}\right)\left\{\frac{2 - M^2}{2(1 - M^2)}K_0\left[\frac{cr}{(1 - M^2)^{1/2}}\right]\right.$$
$$\left. - \frac{M^2}{2(1 - M^2)}K_1\left[\frac{cr}{(1 - M^2)^{1/2}}\right]\right\} \quad M < 1$$

Where:

- $c = \frac{v}{2\alpha}$
- $K_i = modified\ Bessel\ function\ of\ second\ kind\ of\ order\ i$

Starting by this Analytical model a Fem model is therefore proposed to asses and calibrate experimental boundary condition influence in order to validate experimental results which are strongly dependent by test set-up and ambient. In addition for high laser modulation frequencies there can be non linearities and resonance phenomenon that should be avoided. In the absence of any other study on residual stresses of welded joint a numerical model helps to asses every variable and permits to link causes and effects during the studies of the test's results. [8], [9]

Numerical Simulation of Cattaneo Vernotte model

Starting from the Cattaneo Vernotte formulation for heat transfer

$$q + \tau_{CV} \frac{\vartheta q}{\vartheta t} = -k\nabla T$$

Then we can define is for Temperature field

$$q + \tau_{CV} \frac{\vartheta q}{\vartheta t} = -k\nabla T$$

Where

- a thermal diffusivity
- t_cv is relaxation time

in literature t_s has value between 10^-8 and 10^-12.

The relaxation time is definte as

$$\tau = \frac{3a}{v_s^2} = \frac{a}{s^2}$$

.

Where

- v_s is the sound's speed
- s the thermal wave speed

The physical meaning of the relaxation time has slighty different meaning in the two models: Cattaneo Vernotte ,Thermo Mass from which this formulas have been kept [10]

Then we obtain the discretized equation

$$\boldsymbol{M}\ddot{u}_i + \boldsymbol{D}(u_i) + \boldsymbol{K}(u_i) = \boldsymbol{F}_i$$

That can be used to create a Matlab Fem model following the theoretical method proposed in [11]

Then the tested Fem model[12]–[21] is configured as in the following picture

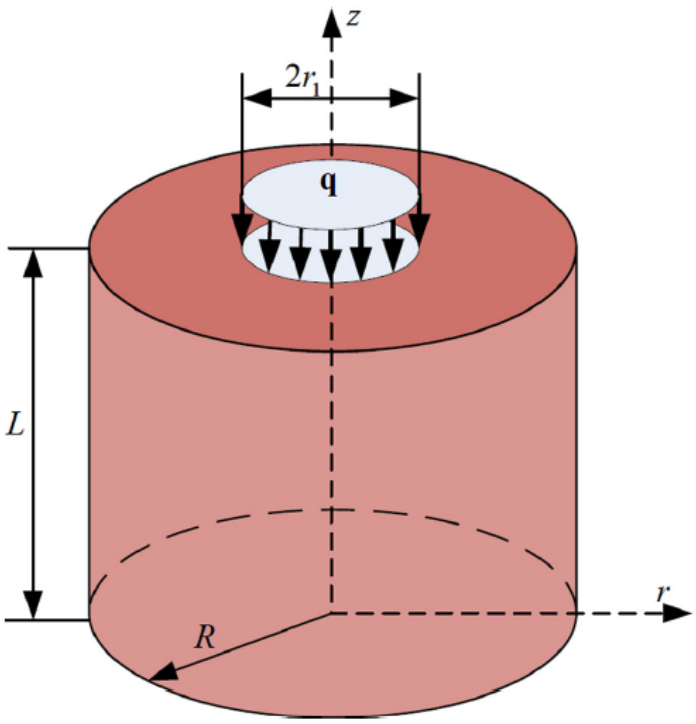

Fig. 1. Cylinder configuration.

With robin B.C.s on all sides and cylindrical cohordinates

The algorithm is presented as proposed in [11]

Initialization

1. Initialize nodal displacement: $\mathbf{u}_i = \mathbf{u}_{i-1} = 0$
2. Initialize the chosen time step size
3. Apply load for the first timestep: forces $\mathbf{F}_i \leftarrow \mathbf{F}_0$
4. Obtain the damping matrix $\mathbf{D}_i$ and stiffness matrix $\mathbf{K}_i$ ($\mathbf{D}_i$ and $\mathbf{K}_i$ keep invariable for linear system)

Precomputation stage

1. Load mesh and boundary conditions
2. Select perfect values of p, q and r according to model's physical property and time step size. Compute and diagonalize the matrix $\alpha M = pK_0\Delta t^2 + \frac{q}{2}D_0\Delta t + rM$ (if the system is linear, then $K_0=K_i$, $D_o=D_i$).

Time stepping

1. Take element nodal displacement u_i and u_{i-1} from previous time step
2. Perform the proposed explicit integration method:
3. Evaluate internal force K_i (u_i) and damping force D_i (u_i).
4. Obtain the external force F_i
5. Obtain the current displacement $\mathbf{u}_{i+1}$ by solving the equation, $\alpha M u_{i+1} = \Delta t^2\left(F_i - k_i(u_i)\right) + D_i\Delta t(u_{i-1} - u_i) + \alpha M(2u_i - u_{i-1})$
6. Update nodal displacement u_i and u_{i-1}

The parameter used are the one suggested in the paper[11]

- p=1/2
- q=2
- r=2

Pulsed Calibration

The input data are

```
radius=3.2; % raggio laser
height=1; % spessore
width=7.5-radius; %raggio del cilindro meno il raggio del laser
Text=23; %indoor temperature [oCta]

MatDensity=3210*1e-9; %[kg/mm3]
MatTherCond=40*1e-3; %[W/mmK]
MatSpecHeat=700; %[J/kg K]

AirAlfa=50*1e-6; %[W/mm2 K]


q=0.4*50/(pi()*radius^2)/MatDensity/MatSpecHeat; %[W/mm2]  Robin B.C.
T_period=0.05; %time interval of the simulation
dt=1e-4; %discretization time step

tau=1e-8;
```

Then the result is compared with a real pulsed test In some cases the results of the simulation shows a good behaviour, in other cases some assessment are needed to take into account the gaussian shape of the laser.

In the picture we can see how

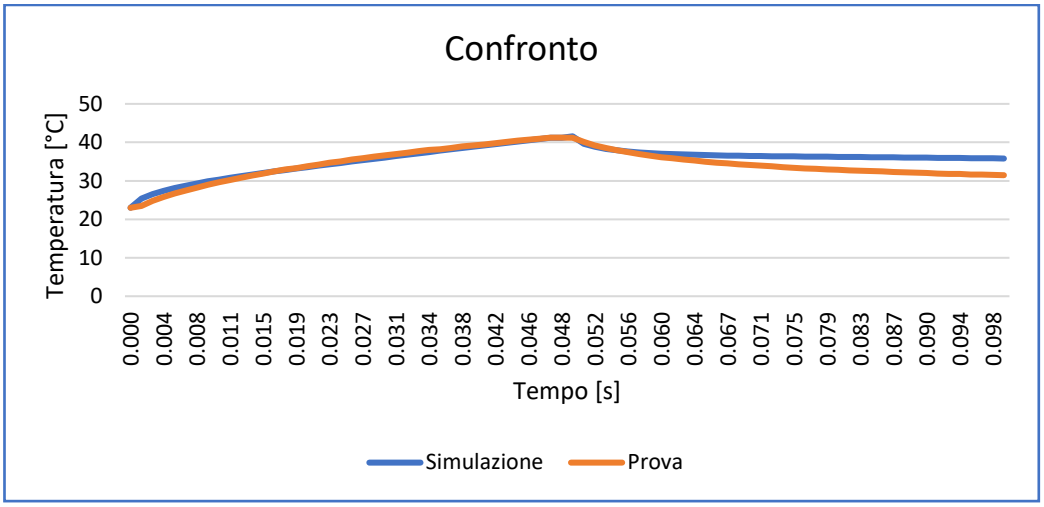

More test to calibrate the model are needed, one of the main future application can be to investigate the diffraction phenomena and thermal resonances by means of modal analysis

Comments

Can be seen from the graphic representation an high instability which have a period about 0,1seconds. This happens because an purposely **incorrect** time constant has been used to be able to see the goodness of the simulation, so if it is taking into account the finite heat propagation speed. This can also be seen in the video of the thermogram.

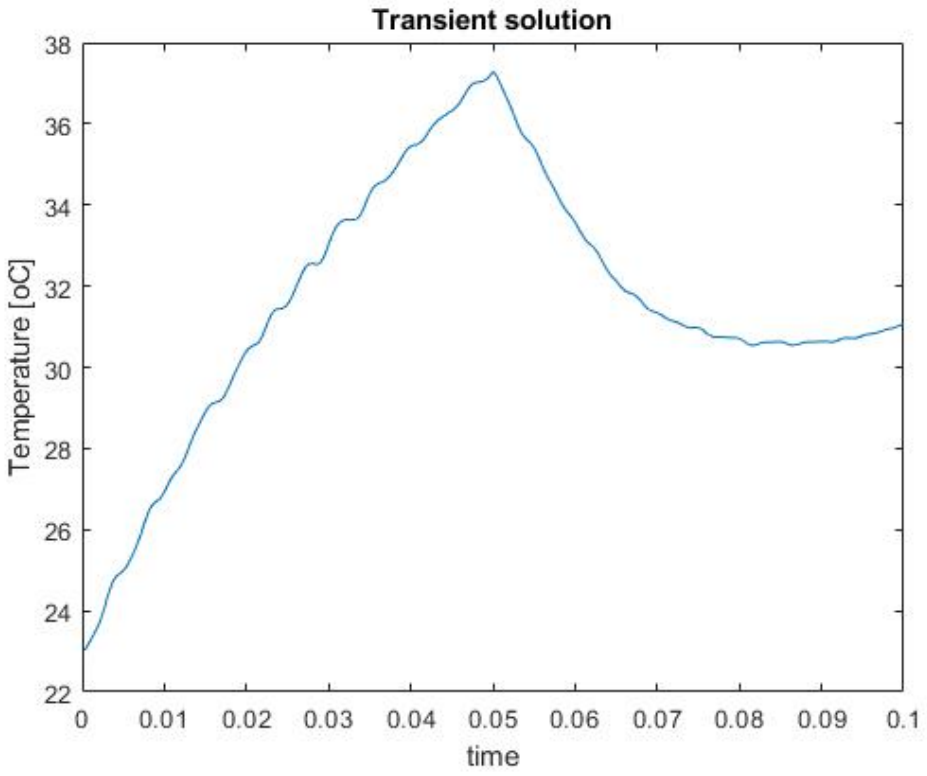

Furthermore the FEM model can be improved to investigate the presence of thermal resonance phenomena during high frequency lock-in tests. No studies seems to exists about this application on steels.[8], [14], [21]–[24]

Materials

The specimen has been cutted starting from a 30mm thick slab. Then two different type of butt weld has been done. The first specimen has been made using the correct technique to avoid the presence of residual stresses while the second one has been made such a way to induce the presence of residual stresses.

The main geometric characteristics of the specimen are therefore presented:

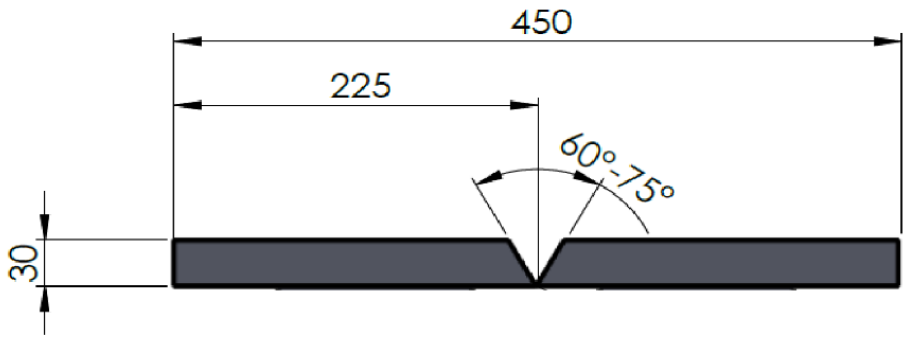

The ‘without residual stresses’ specimen welding specification are:

- Preheating 80°C
- String bead
- Root gap 1-2 mm
- Postheating 400-450°C x 1 h
- Insulated cooling

While the ‘with residual stresses’ specimen welding specification are:

- NO preheating
- Wave bead
- Root gap 2-3 mm
- High current level
- Waterwash cooling

Equipment

The Thermal camera used for all the tests is a FLIR A6751sc shown in the picture.

The laser head is controlled with the software MultiDES, and the thermogram are recorded and exported with the software ResearchIR.

Exporting the thermogram recording as .csv files some parameter are requires for the calibration

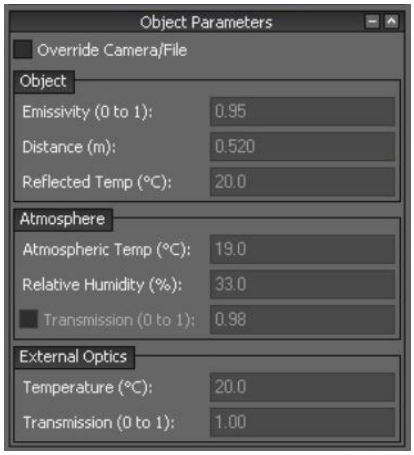

These are the most important and a correct calibration must be done, in particular the emissivity varies a lot between different type of coating and surfaces and needs to be assessed. In the following chapter this will be done. The reflected temperature is measured by mean of a metallic reflective element and is calibrated on field. As long we work with specimen which are not at high temperature the reflect temperature is usually near to the environmental temperature. The other parameter can be easily measured from a thermometer present in the room.

Assessing emissivity

The most important parameter to assess when performing thermographic test is the emissivity. This can be kept from standard table or tested in lab.

In this work we tested it in the lab.

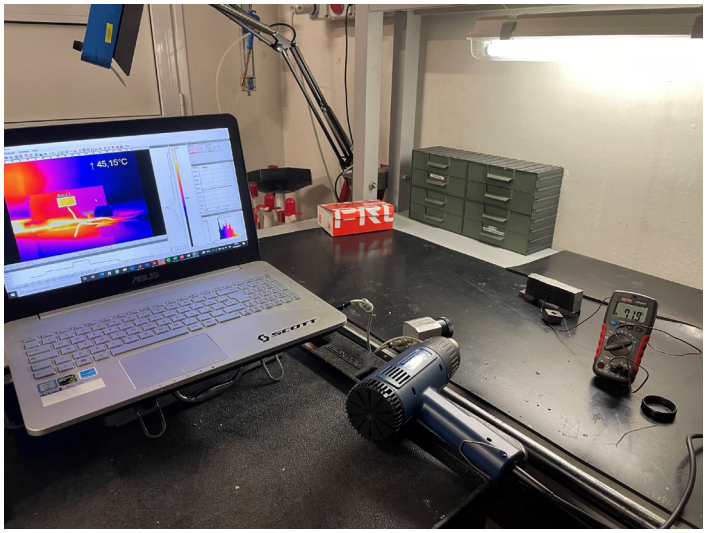

The experimental set-up has this parameter:

- T enviroment : 23.1°C
- Distance Thermocamera-Specimen : 29cm

Then by mean of a thermocouple the temperature is measured and recorder while the specimen is excited by mean of a phon.

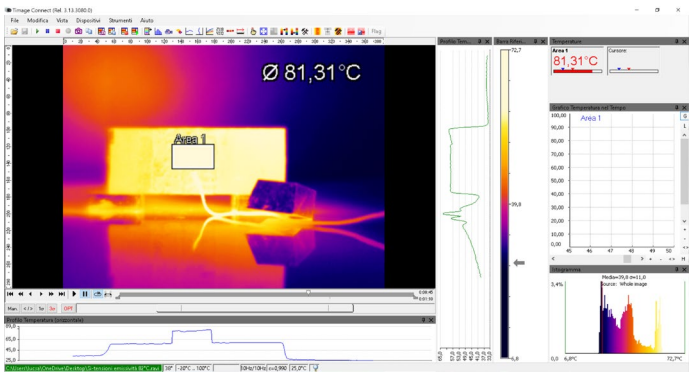

Finally through the TImageConnect Software is possible to reverse assess the emissivity.

In both cases the emissivity obtained is **0.55**.

Pulsed

The pulsed thermography, also called Transient Infrared Thermography (TIRT), is an active thermography technique. The heat source has to be capable to reach high power in short period. The impulse duration usually last few milliseconds to 5 seconds and depends by physical and geometrical properties of the investigated component

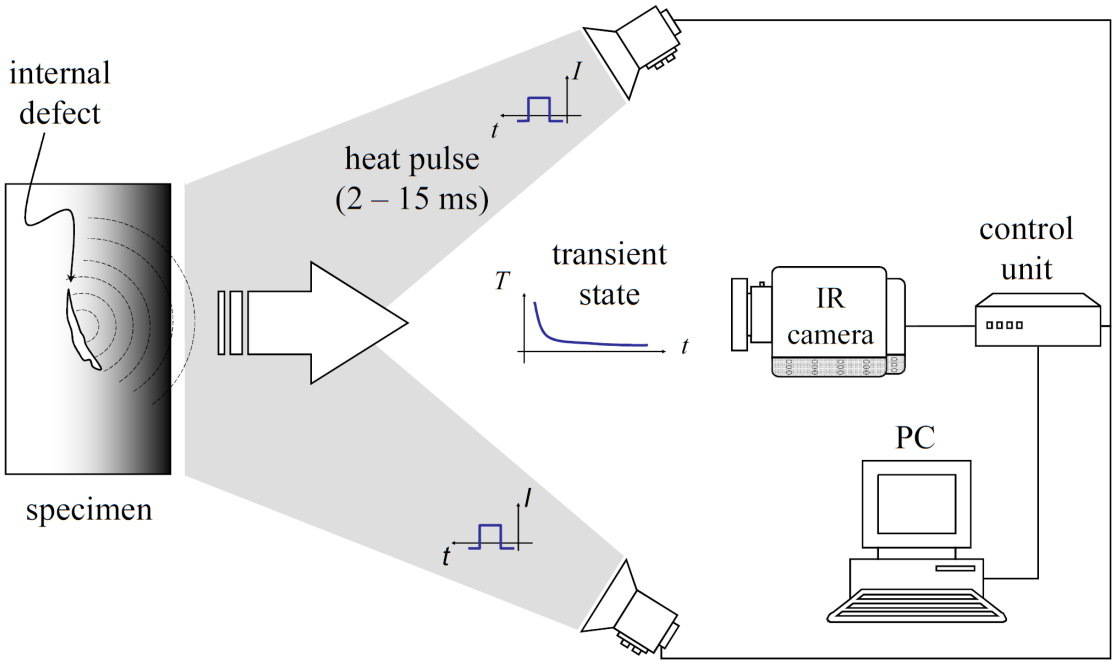

One of the main issues about the use of pulsed thermography in welded joints is the highly dependence by the surface parameter. The presence of different thickness of the coating in the investigated zone or even the of small corroded zone can alterate the thermogram shape Furthermore no information about anisotropy can be extracted.

Preliminary study

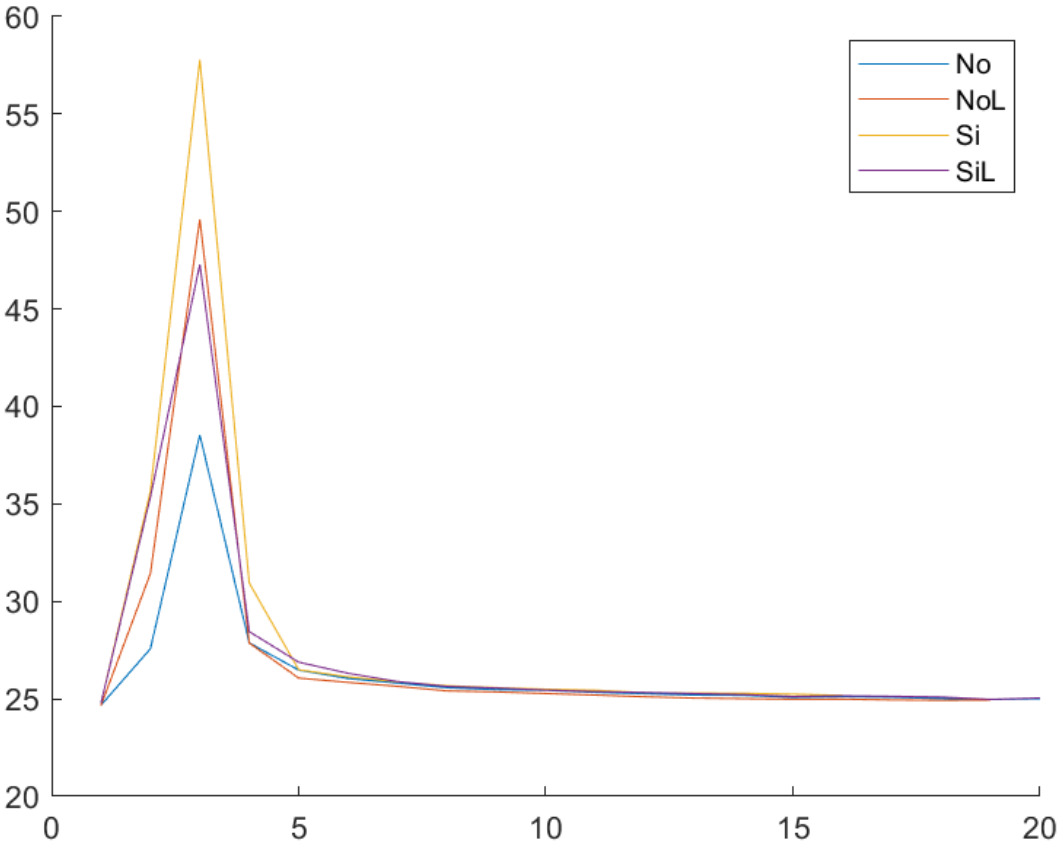

A Preliminary study has been performed to check the repeatability of the analysis.

Each curve plotted in the graph is obtained by averaging 4 different tests

Is possible to see that NoL and SiL curves which represent the response in the base material show the same behaviour while there is a really different behaviour between the two weldings with and without residual stresses. This can be related to microstructure and to the photo-thermal characteristics of the surface, but we don't know how the contribution can be weighted.

[25]–[29]

Pulsed Calibration

Once knew the entity and the type of impulse, and what kind of behaviour to expect s additional test have been performed. The scope of this test has been to study the cooling curve shape to characterize the material. To improve the precision high frame rate has been chosen. As first guess the Newton law of cooling can be used, however we can only extrapolate the time constant, but no more information can be catch from this value. While considering the convective constant the same for all the tests, we cannot explain the cooling only considering the heat losses with the air, but we have also to consider conductive phenomena inside the bulk of the material. So this method can be used as first guess to find a different thermal behave of the investigated material.

Acronym:

Y-RS = Yes Residual Stresses

N-RS = No Residual Stresses

Base Metal	NO-RS	1000ms	50%	50 fps

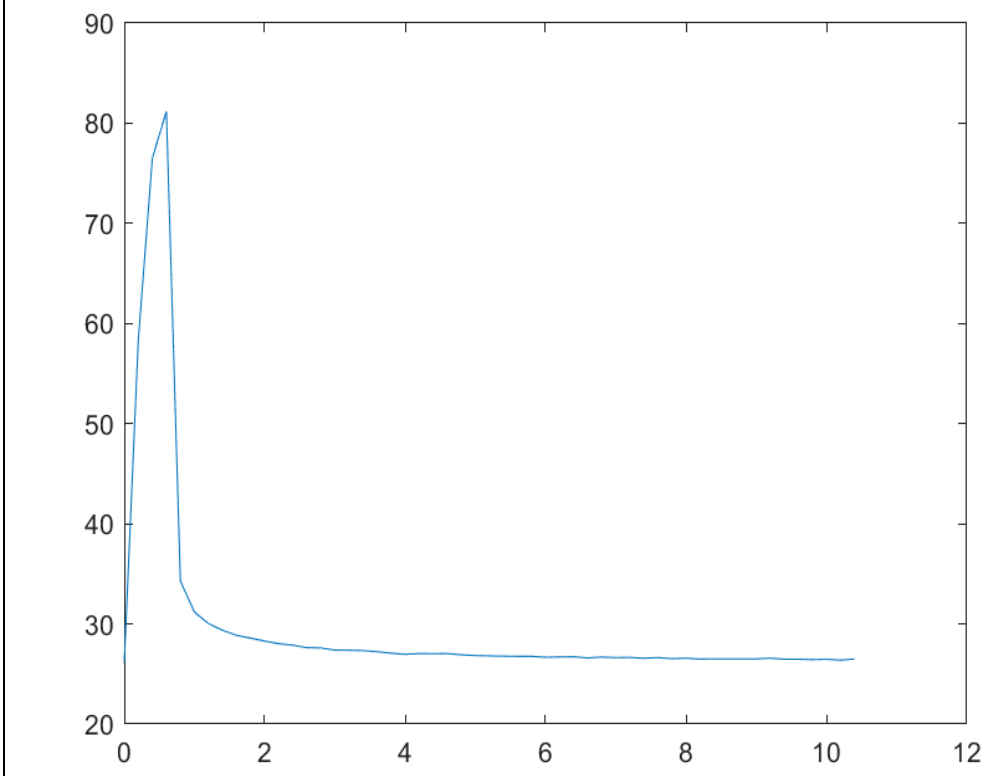

Base Metal	NO-RS	10000ms	25%	12.5 fps

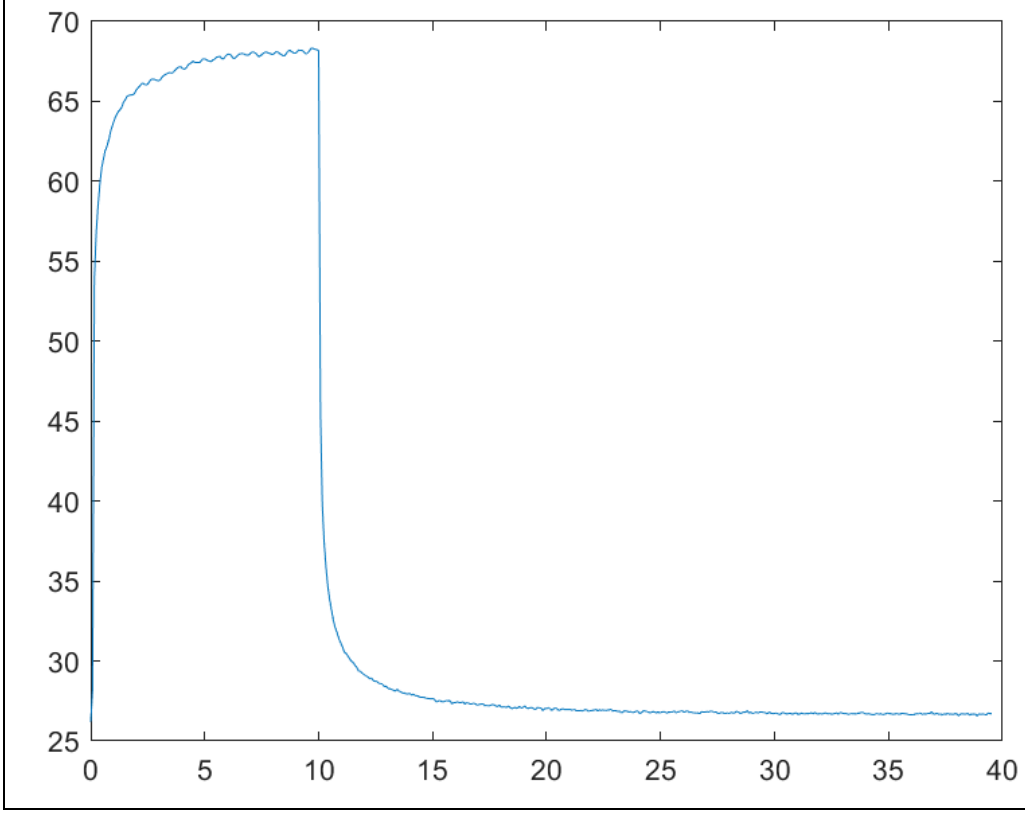

Weld Bead	NO-RS	1000 ms	50%	50 fps

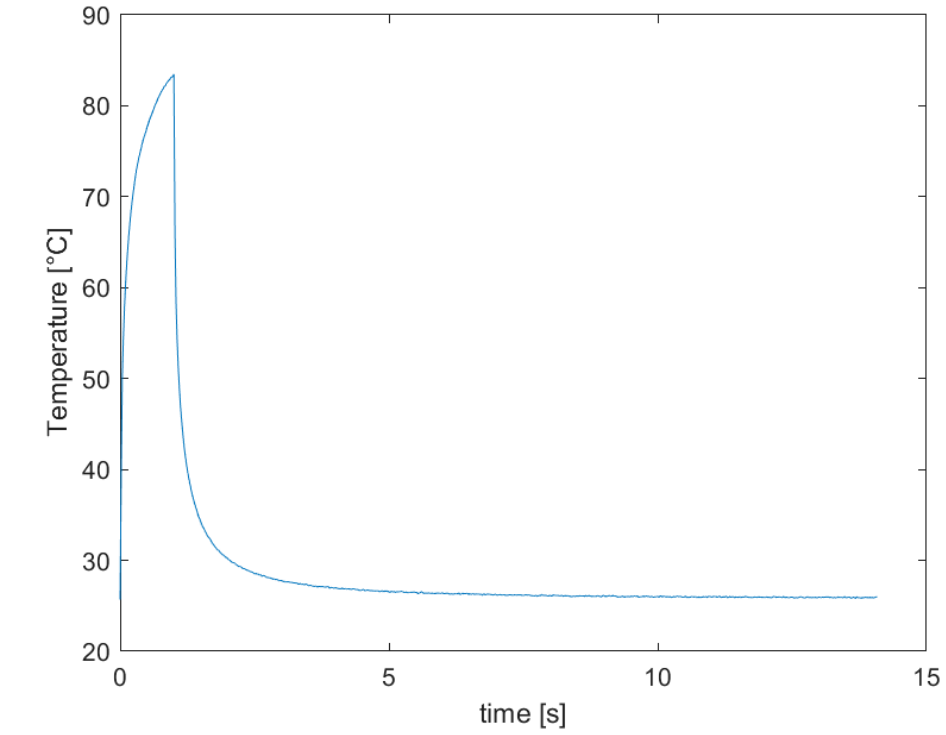

Weld Bead	NO-RS	10000 ms	25%	12.5 fps

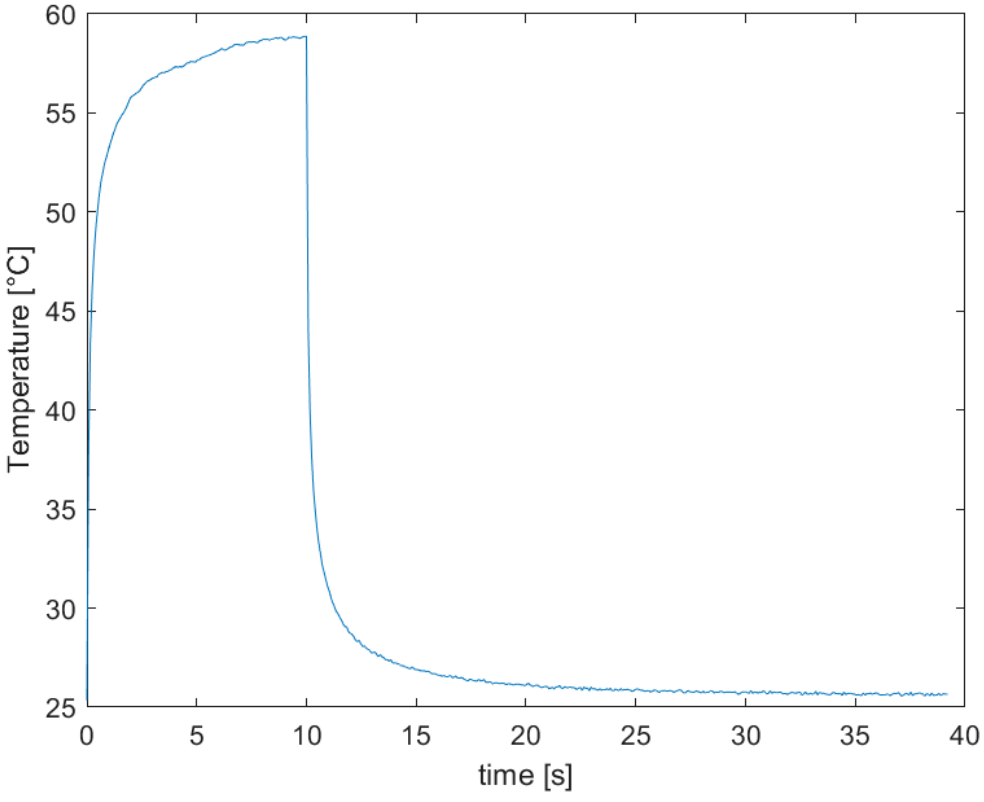

Base Metal	Y-RS	1000 ms	50%	50 fps

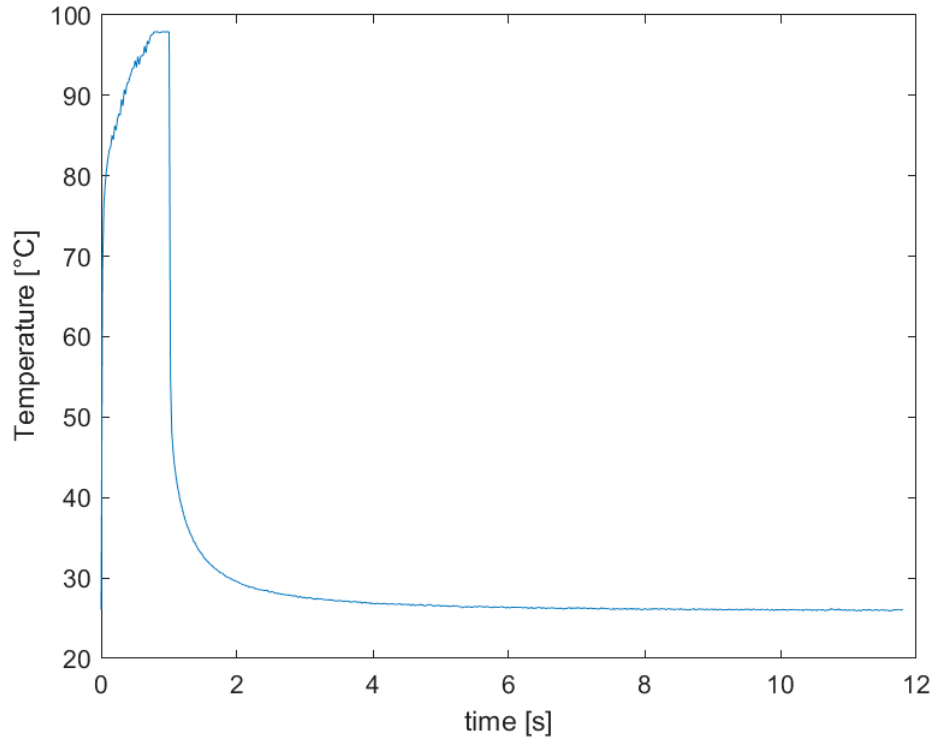

Base Metal	Y-R	10000ms	25%	12.5 fps

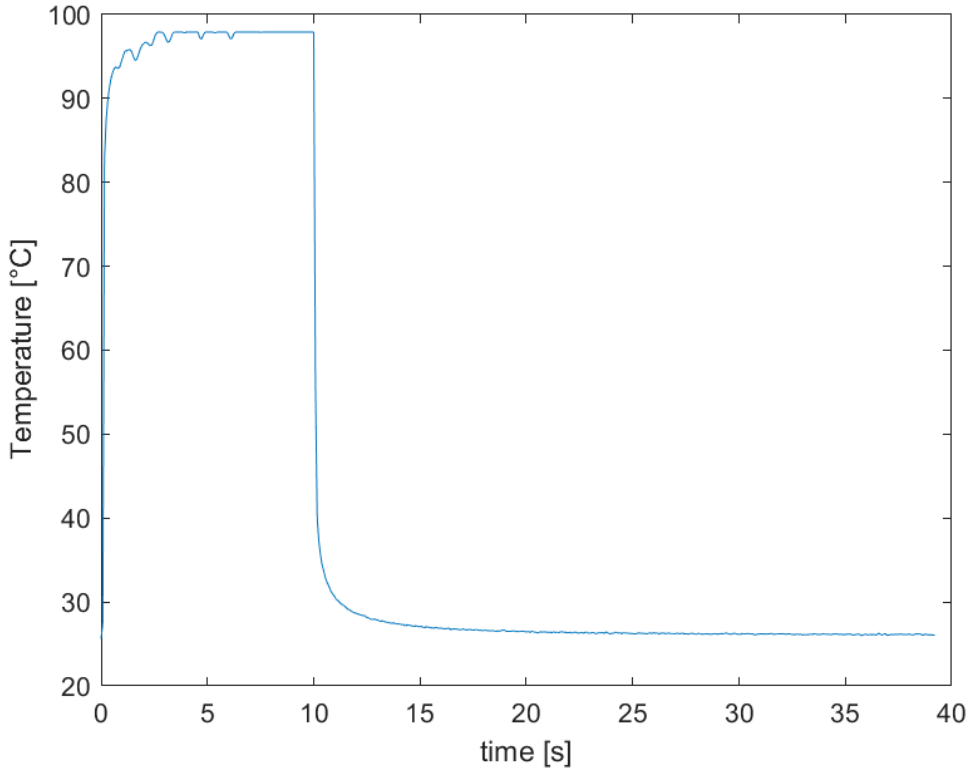

Weld Bead	Y-RS	1000 ms	50%	50 fps

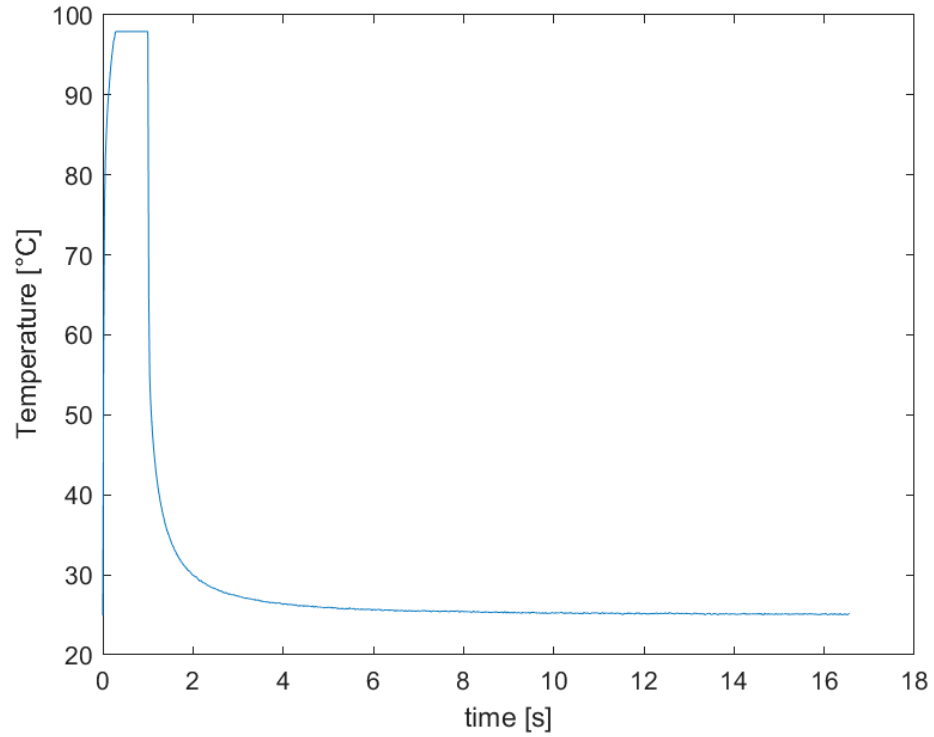

Weld Bead	Y-R	10000ms	25%	12.5 fps

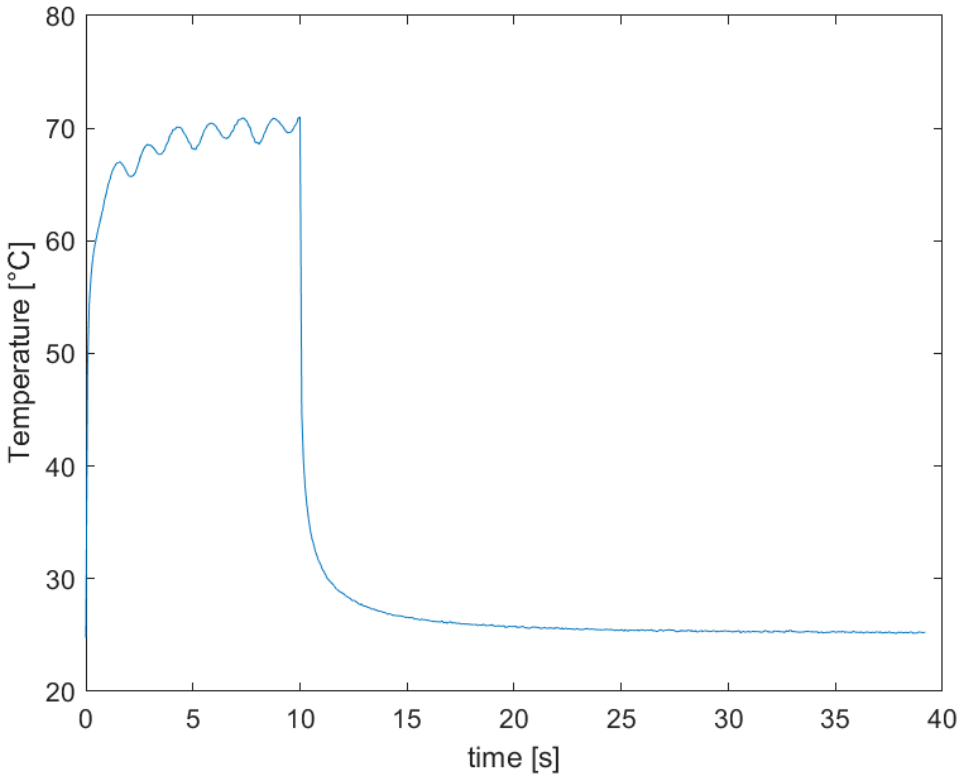

Results and discussion

From the performed tests no more information can be extrapolated than the one in the preliminary studies. An high variability in the tests is present, and only studying the hottest point of the thermogram doesn't work. Furthermore the peak is reached only within the zone of the laser spot, in that zone the heat input has a gaussian distribution, in the particular case of short excitation time we can see how lots of variables are involved and this lead to non repeatable results.

To improve the reliability of this test was tried to extrapolate some shape factor parameter from the exponential decay, so trying to uncouple the the thermogram from the peak temperature which is highly variable, but no consistent and reliable results have been found.

Lock in

Introduction to Lock-in routine

From the experience maturated during the pulsed experimental campaign the need of more liable method arises. Lock-in thermography is widely used in literature applied to lamp exciter, and even to laser beam exciter. In addition a oscillatory signal is easier to analyse and to denoise. This work will focus on the phase method, anyway other methods are commentated in the state of art chapter.

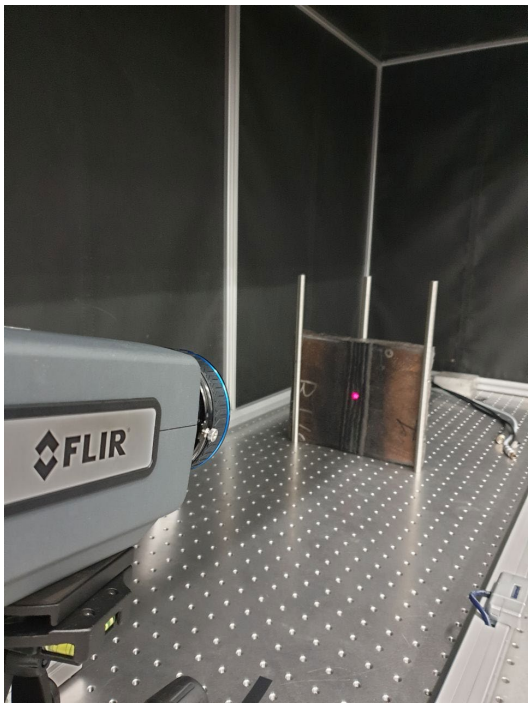

The most common method to extract the phase of the signal is to use the fast fourier transform. This is applied by meant of the fft command of Matlab analysing the signal with this algorithm, that is a 1D fourier transform applied to each pixel. The data are formatted as a tensor of 3 dimension where the first two are the spacial dimensions (pixel) and the third dimension is the time dimension (frames) .[2], [3], [28]–[34]

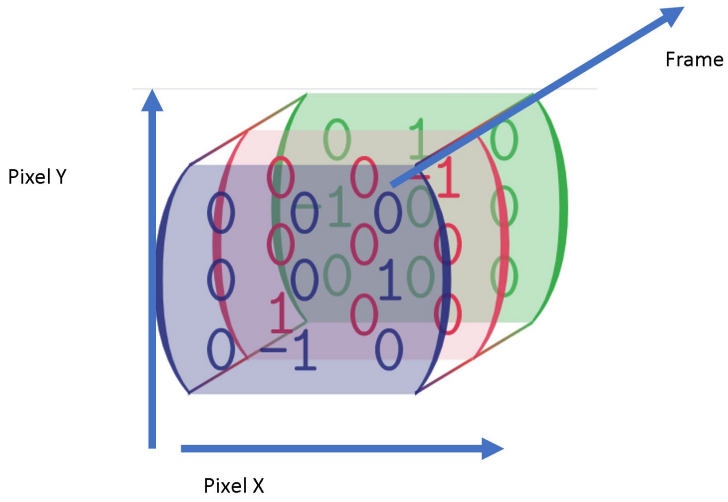

However this method is computational heavy, require times and data space on the pc. So another method based on the lock in amplifier is here proposed.

$$y = Y * \cos(\omega_1 t + \phi)$$

$$x = X * \cos(\omega_2 t + \phi)$$

$$x * y = \frac{X * Y}{2} * \cos\big((\omega_1 - \omega_2) * t + \phi\big) + \frac{X * Y}{2} * \cos\big((\omega_1 + \omega_2) * t + \phi\big)$$

$$\omega_1 = \omega_2 \quad - \quad Y = 2$$

$$x * y = X * \cos(\phi) + X * \cos(2\omega * t + \phi)$$

Neglect the contenta t 2omega by means of low pass filter or zeroing the signal and considering only the mean value of the result to extract S.

$$x(t) = A * \cos(\omega * t + \phi)$$

$$c(t) = 2 * \cos(\omega * t)$$

$$s(t) = 2 * \sin(\omega * t)$$

$$S = A * \cos(\omega * t + \phi) * 2 * \cos(\omega * t) = A * \cos(\phi) + A * \cos(2 * \omega * t)$$
$$= A * \cos(\phi)$$

$$C = A * \sin(\phi)$$

$$A = \sqrt{S^2 + C^2}$$

$$\phi = \text{atan}\left(\frac{S}{C}\right)$$

This method shows considerably shorter computational times and similar result to the fft method.

The aim of this data processing is to have a liable phase calculation to extract the phase plot along the distance from the laser spot to apply the phase method presented in the state of art chapter. As can bee seen in the following pictures the amplitudes map is more difficult to read and suffer from influence and interference from surface flaws such as local corrosions or irregularities (the weld bead is not flat, but presents some inhomogeneities)

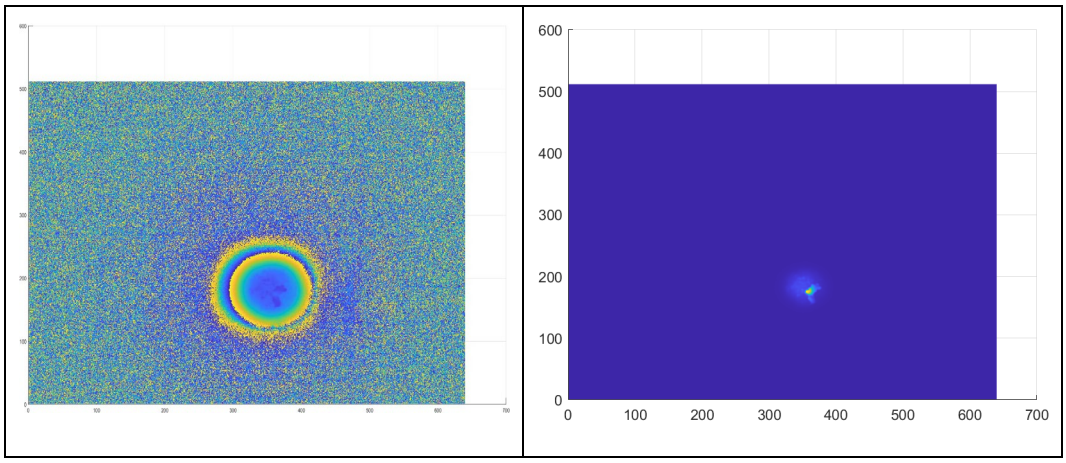

Laser power\harmonics\methods comparisons

- Lock-in: 25 impulses
- Reflection configuration
- Low modulation frequency : 1 Hz
- Distance by the thermocamera: 22.5cm
- Method 1: FFT matlab
- Method 2: lock-in amplifier
- Axis Y: Longitudinal to the weld bead
- Axis X: Orthogonal to the weld bead

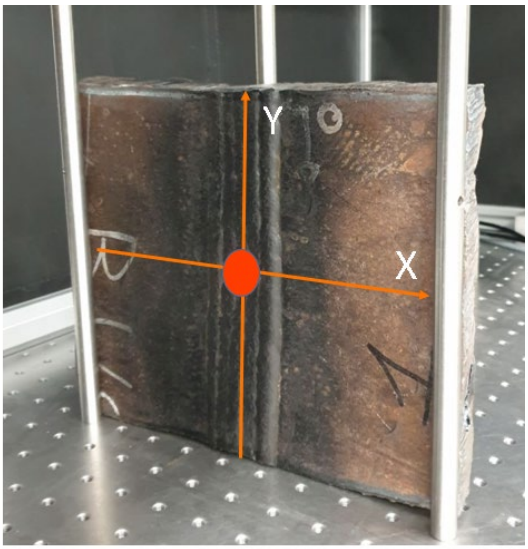

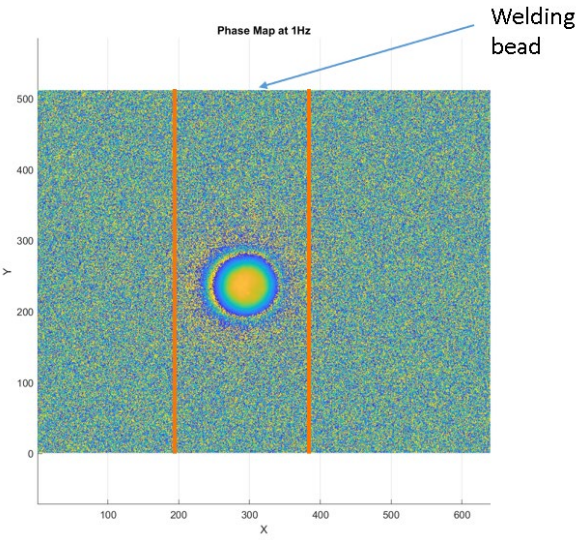

Acronym:

Y-RS = Yes Residual Stresses

N-RS = No Residual Stresses

METHOD 1 Laser Power 11%							
NO-RS	1 HZ	11%	12.5 fps	Y-RS	1 HZ	11%	12.5 fps

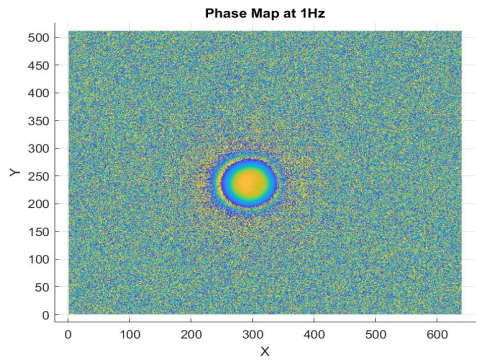

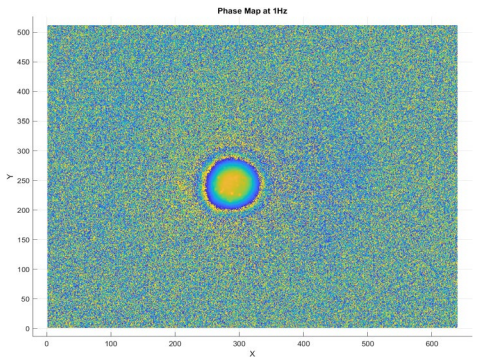

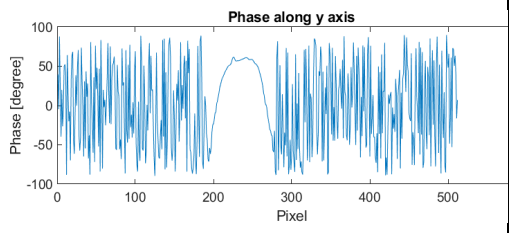

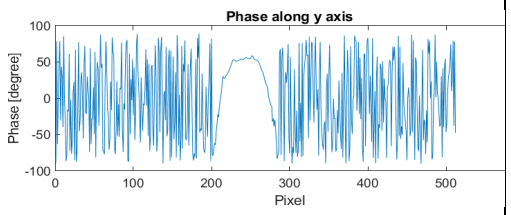

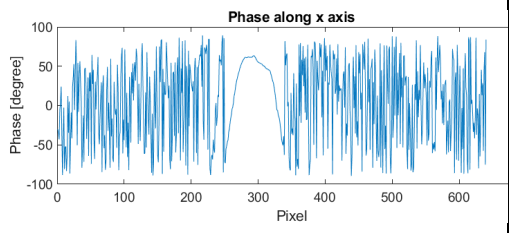

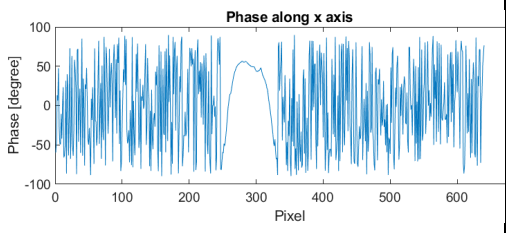

METHOD 1 Laser Power 11%							
NO-RS	3 HZ	11%	12.5 fps	Y-RS	3 HZ	11%	12.5 fps

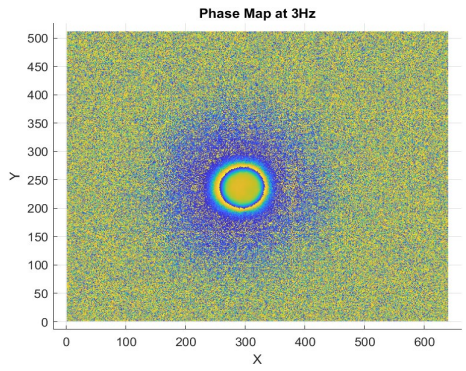

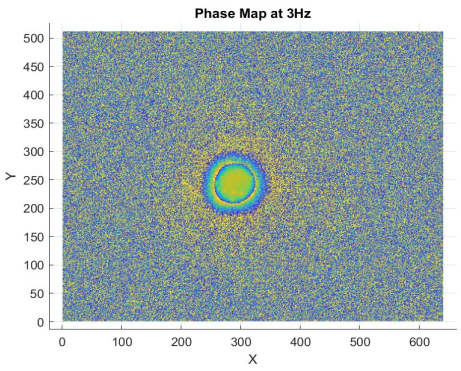

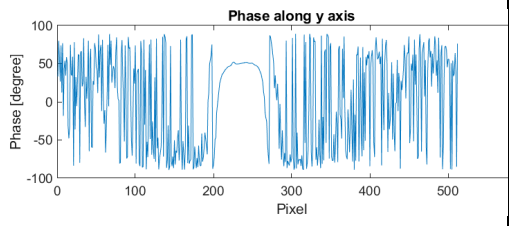

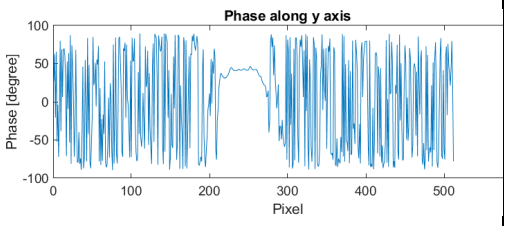

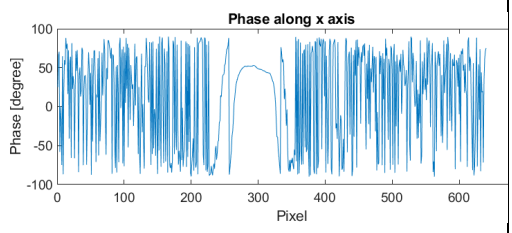

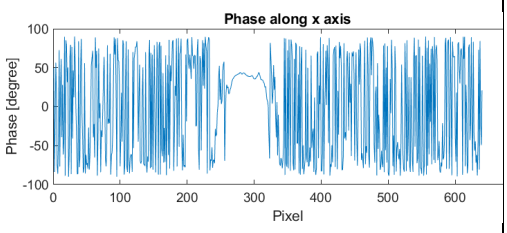

METHOD 1 Laser Power 11%							
NO-RS	5 HZ	11 %	12.5 fps	Y-RS	5 HZ	11 %	12.5 fps

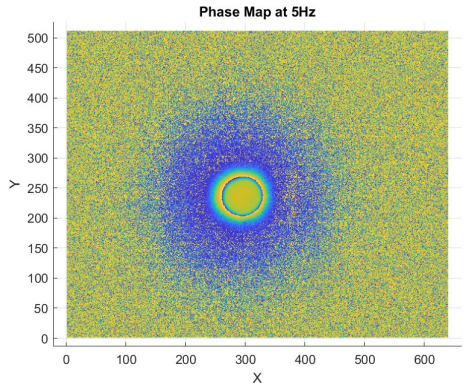

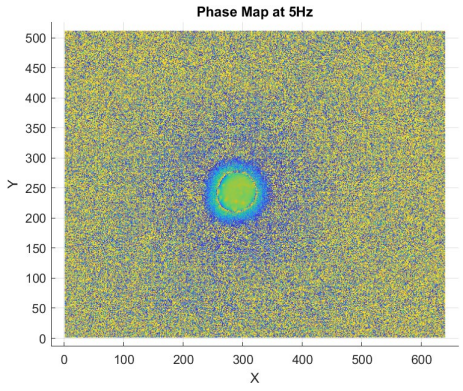

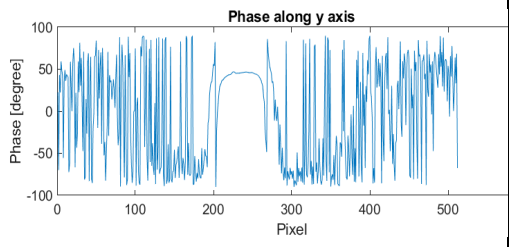

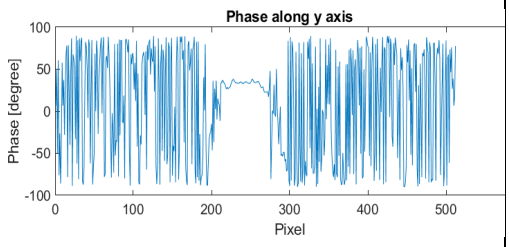

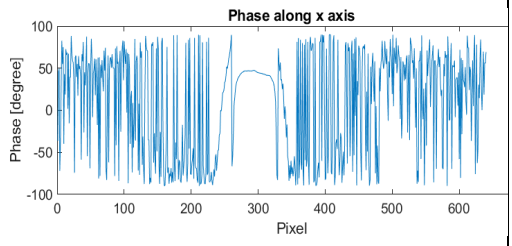

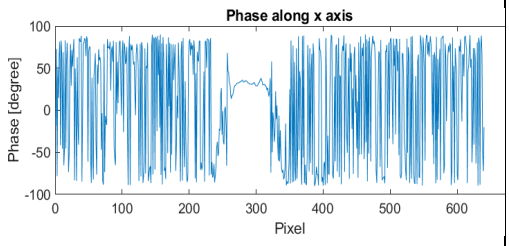

METHOD 2 Laser Power 11%							
NO-RS	1 HZ	11%	12.5 fps	Y-RS	1 HZ	11%	12.5 fps

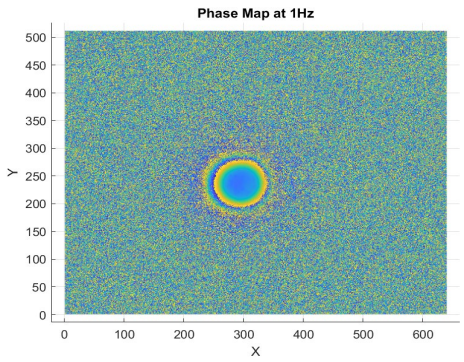

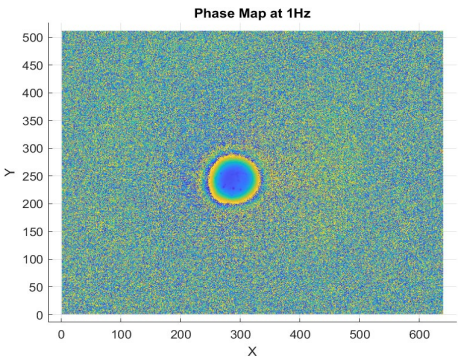

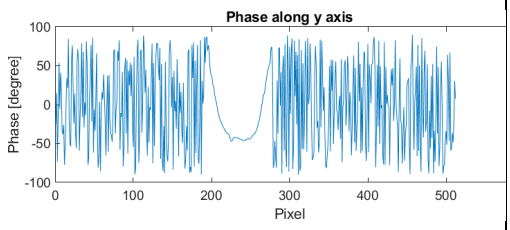

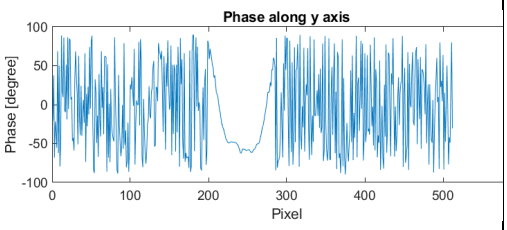

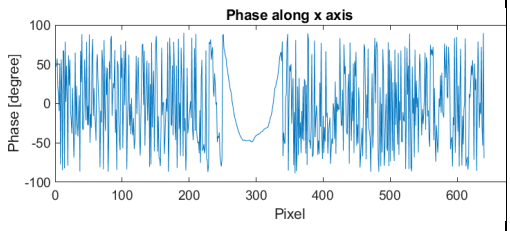

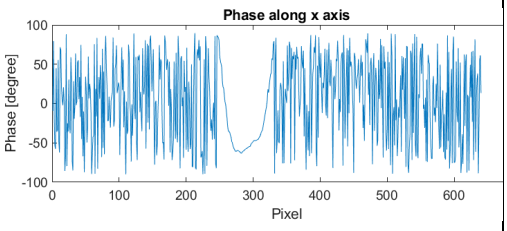

METHOD 2 Laser Power 11%							
NO-RS	3 HZ	11%	12.5 fps	Y-RS	3 HZ	11%	12.5 fps

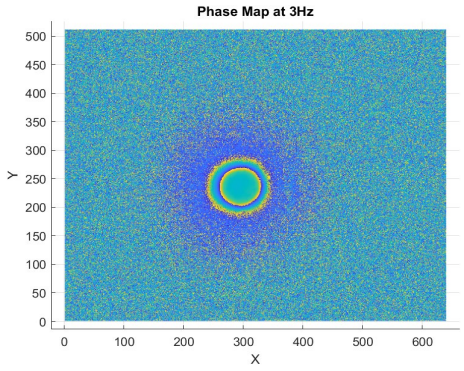

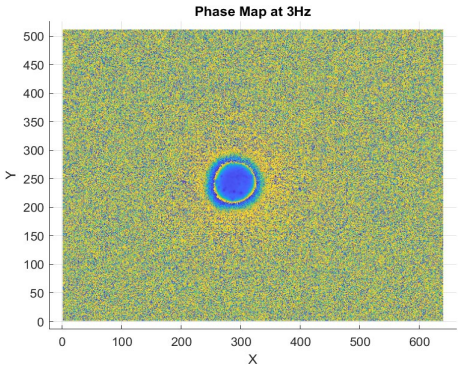

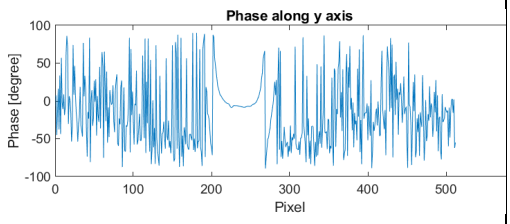

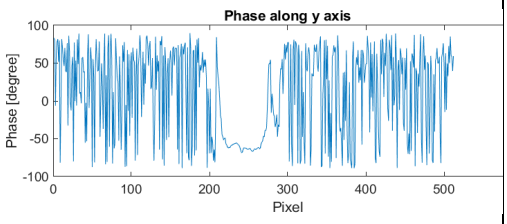

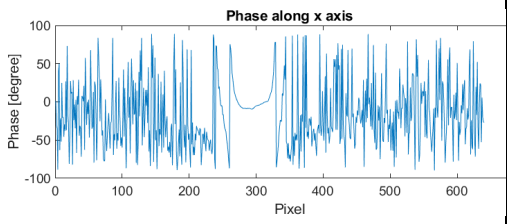

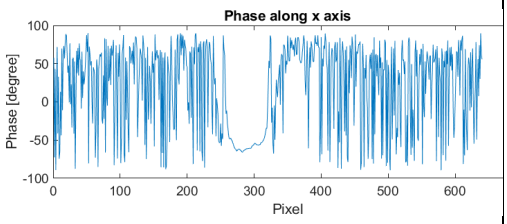

METHOD 2 Laser Power 11%							
NO-RS	5 HZ	11%	12.5 fps	Y-RS	5 HZ	11%	12.5 fps

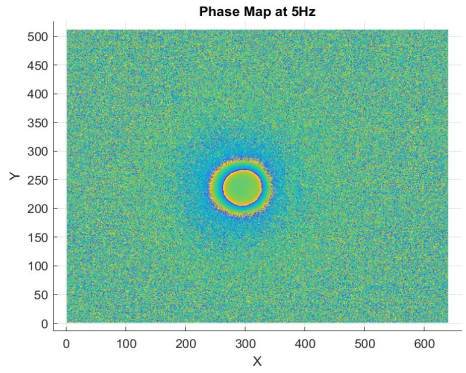

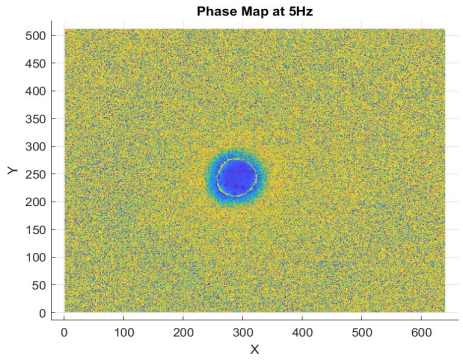

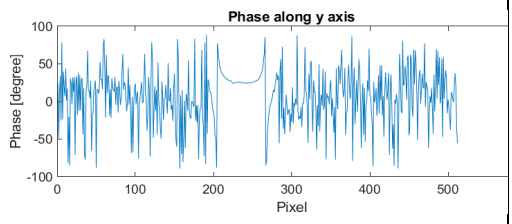

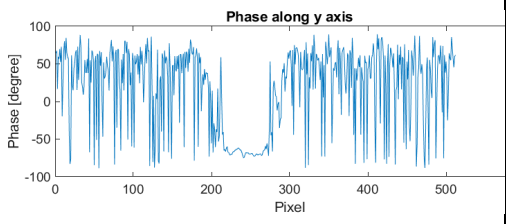

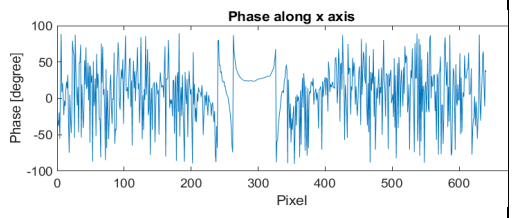

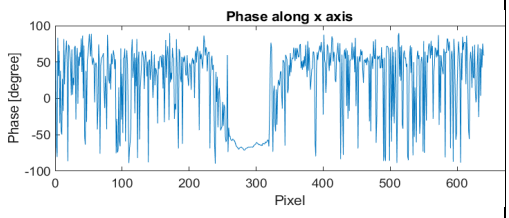

METHOD 1 Laser Power 40%							
NO-RS	1 HZ	40%	12.5 fps	Y-RS	1 HZ	40%	12.5 fps

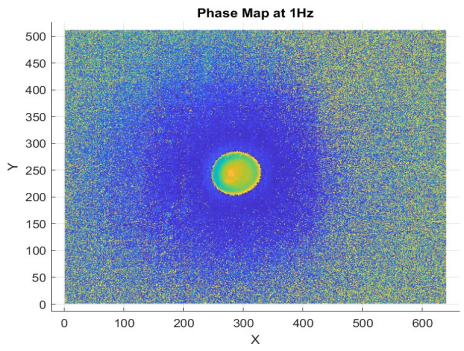

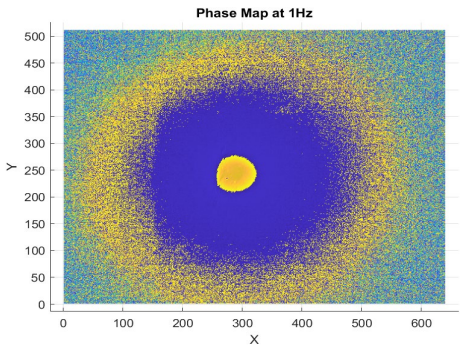

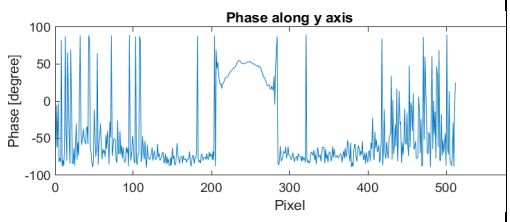

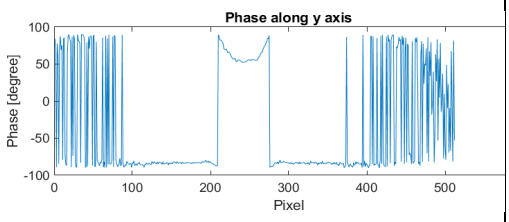

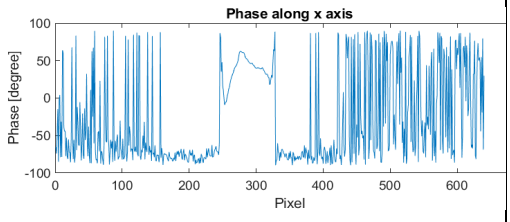

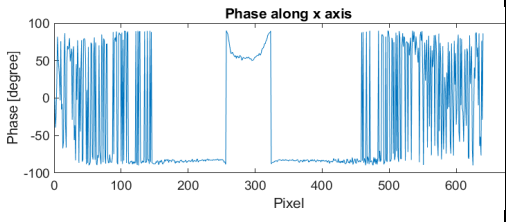

METHOD 1 Laser Power 40%							
NO-RS	3 HZ	40%	12.5 fps	Y-RS	3 HZ	40%	12.5 fps

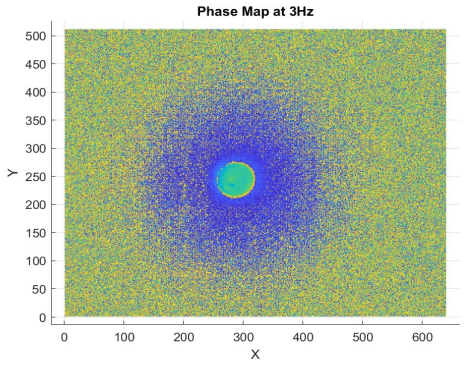

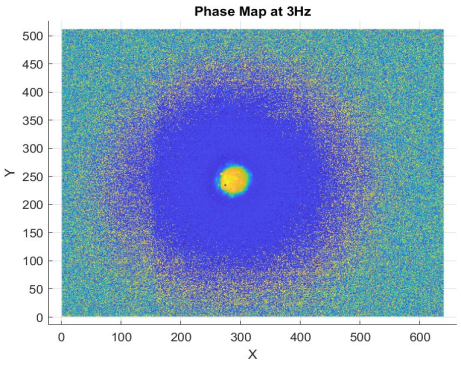

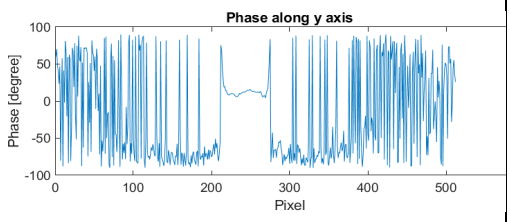

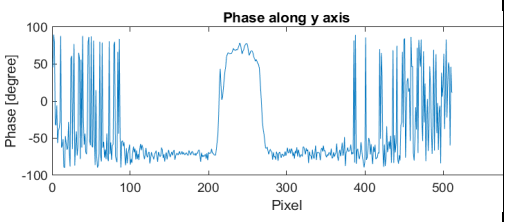

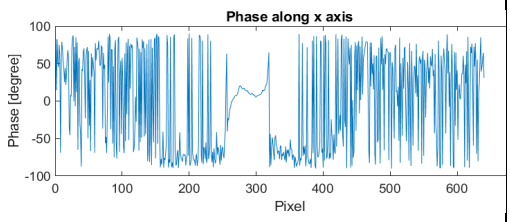

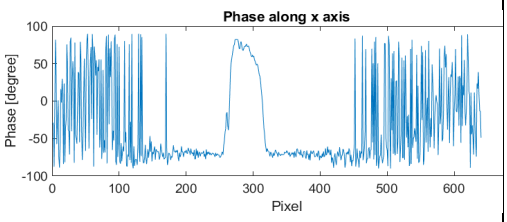

METHOD 1 Laser Power 40%							
NO-RS	5 HZ	40 %	12.5 fps	Y-RS	5 HZ	40 %	12.5 fps

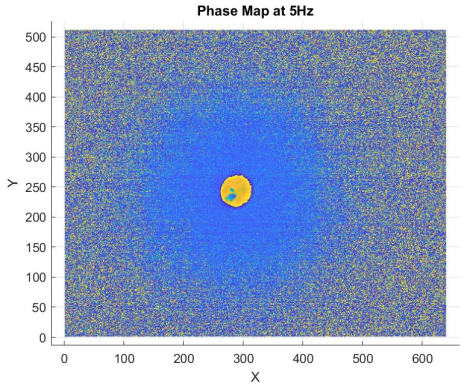

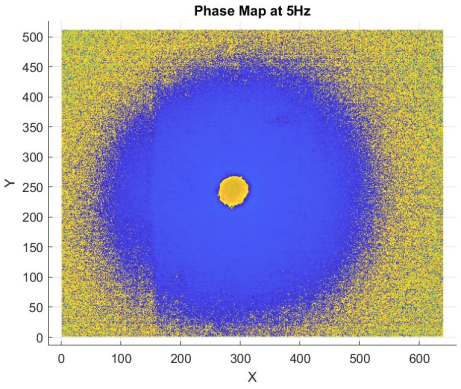

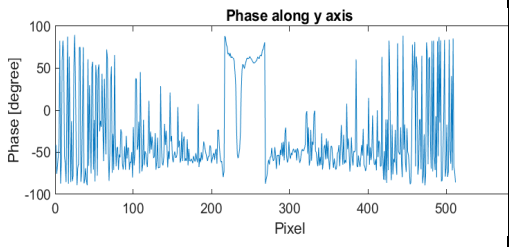

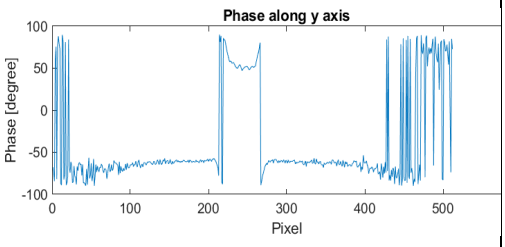

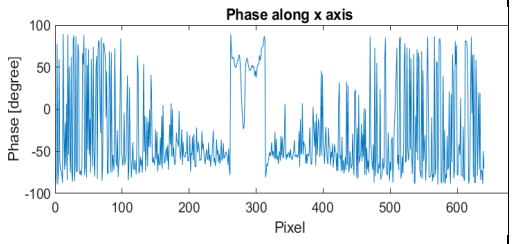

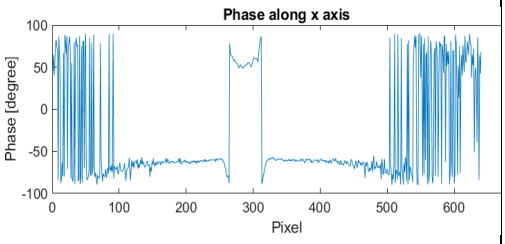

METHOD 2 Laser Power 40%							
NO-RS	1 HZ	40%	12.5 fps	Y-RS	1 HZ	40%	12.5 fps

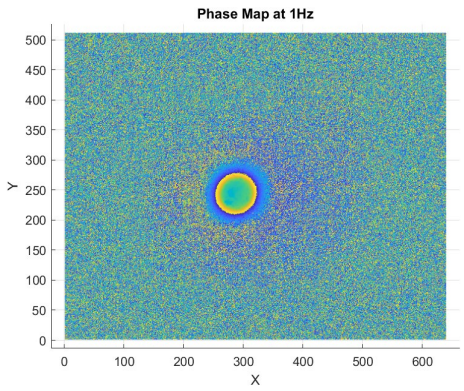

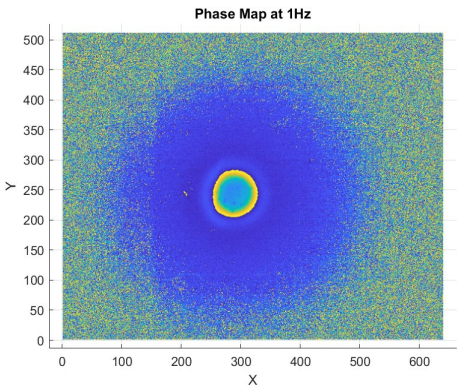

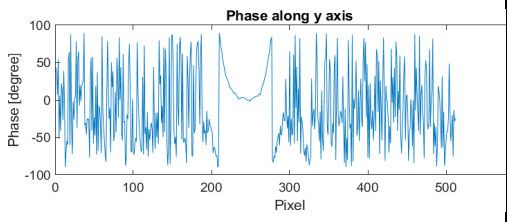

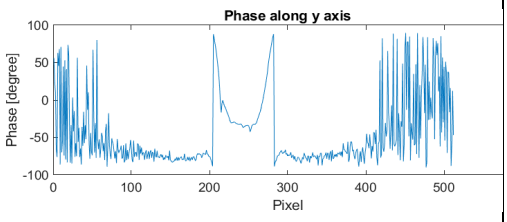

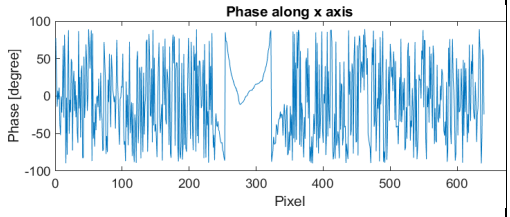

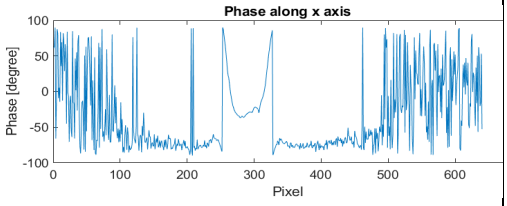

METHOD 2 Laser Power 40%							
NO-RS	3 HZ	40%	12.5 fps	Y-RS	3 HZ	40%	12.5 fps
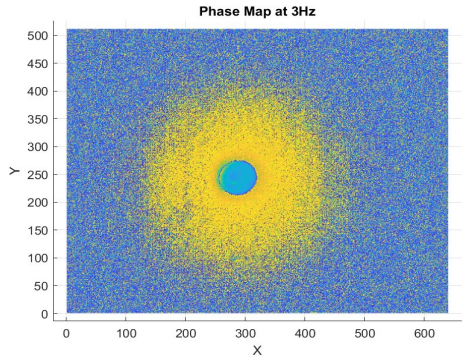				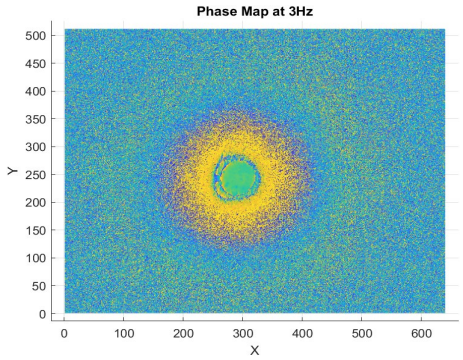			
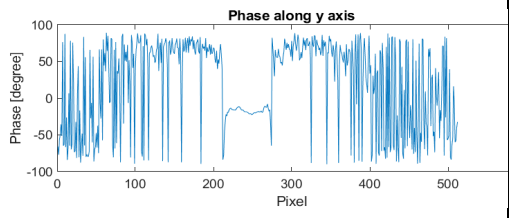				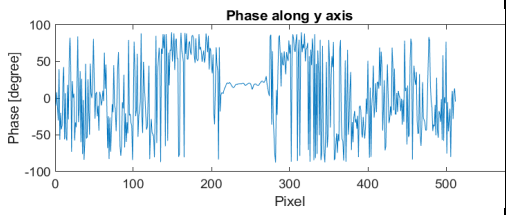			
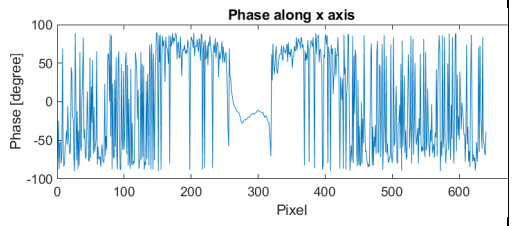				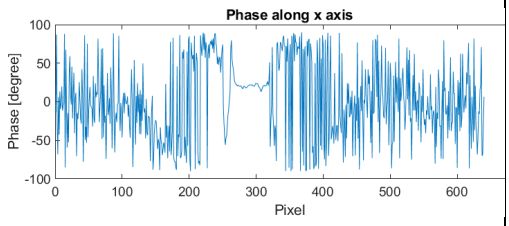			

METHOD 2 Laser Power 40%							
NO-RS	5 HZ	40%	12.5 fps	Y-RS	5 HZ	40%	12.5 fps

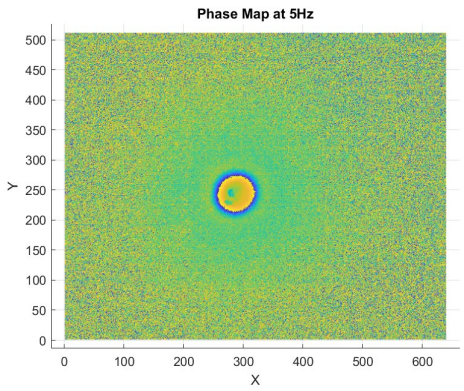

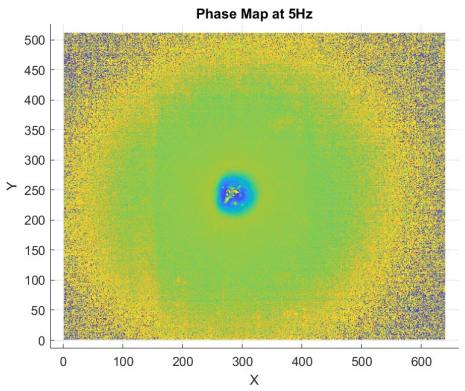

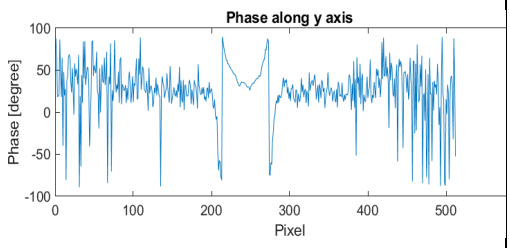

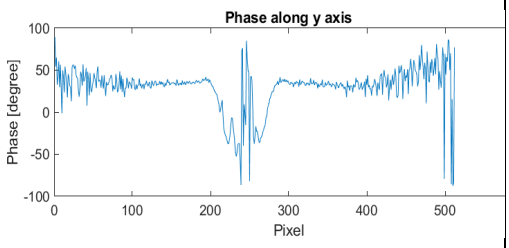

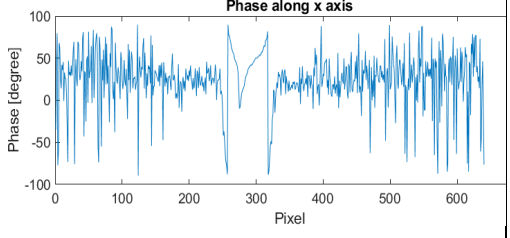

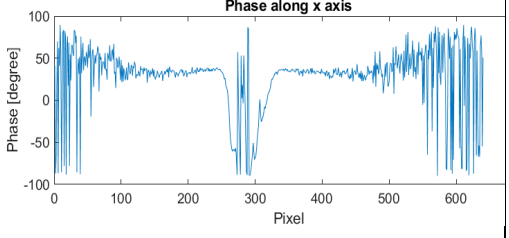

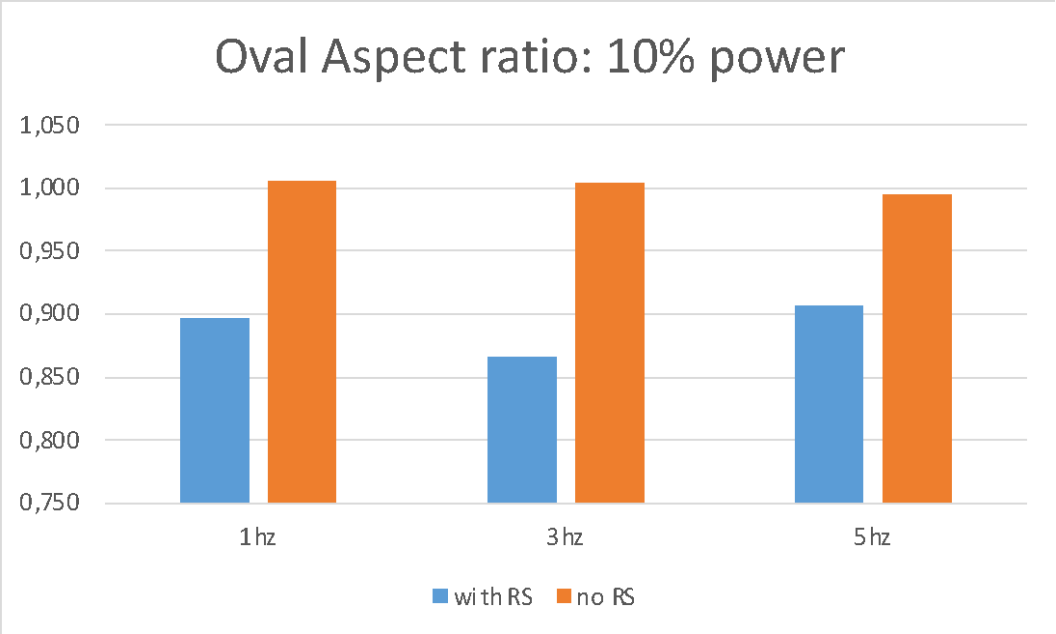

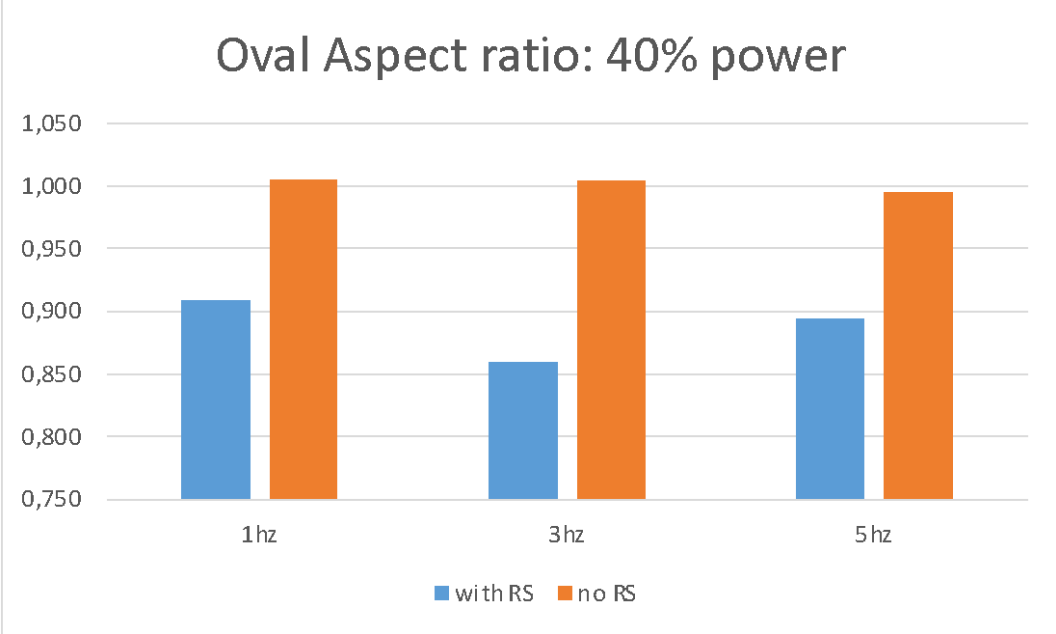

The oval aspect ratio is the ratio between the dimension along the two axis (X,Y) of the radius of the heat spot of the thermogram.

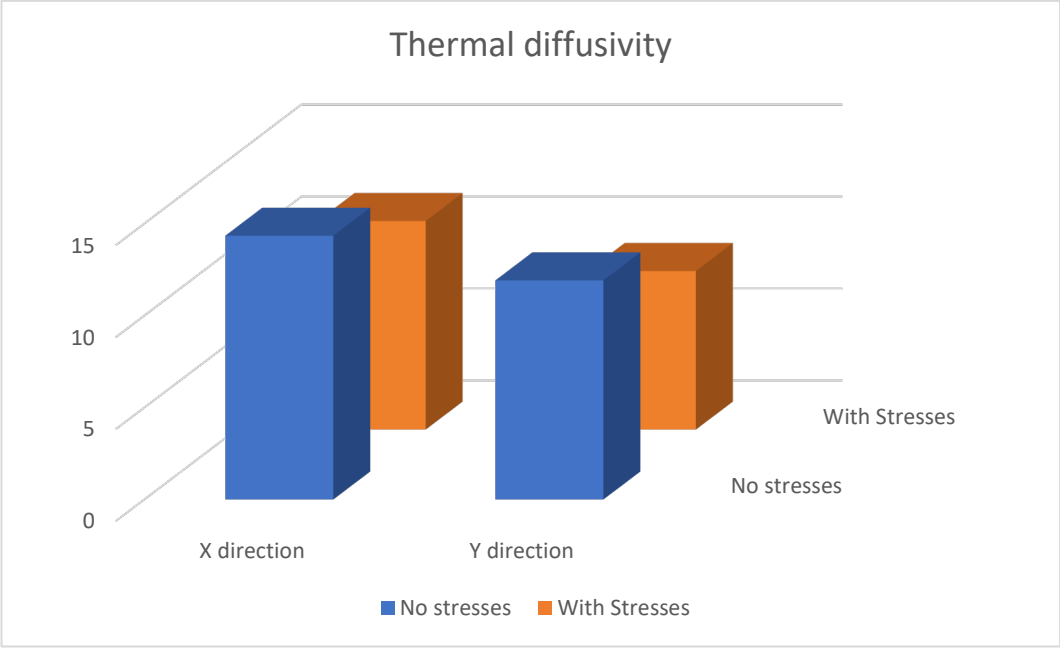

	Thermal diffusivity [mm^2/s]		
	X dir.	Y dir.	X/Y %
No stresses	3.752798	3.117928	120.36
With stresses	2.966974	2.256169	131.50

Base Metal vs Welded joint [With\Without residual stresses]

More test has been performed to investigate the goodness of the calibration of the method, in particular the need borns by the fact that performing laser active IRT on irregular surfaces shows high number of hot spot on the thermogram. This problem is disturbing the goodness of data elaboration, and the readability of phase plot, in particular when working with high power and short period heat impulses.

So has been performed two different kind of test with a period of the impulse of 1000ms and 10000ms with a duty cycle of 50% of the time laser tuned on and 50% off. The lockin frequency of the two test are respectively 1Hz and 0.1Hz.

In this test the X(horizontal) axis will be the one along the welding direction and the Y(vertical) orthogonal to the welding.

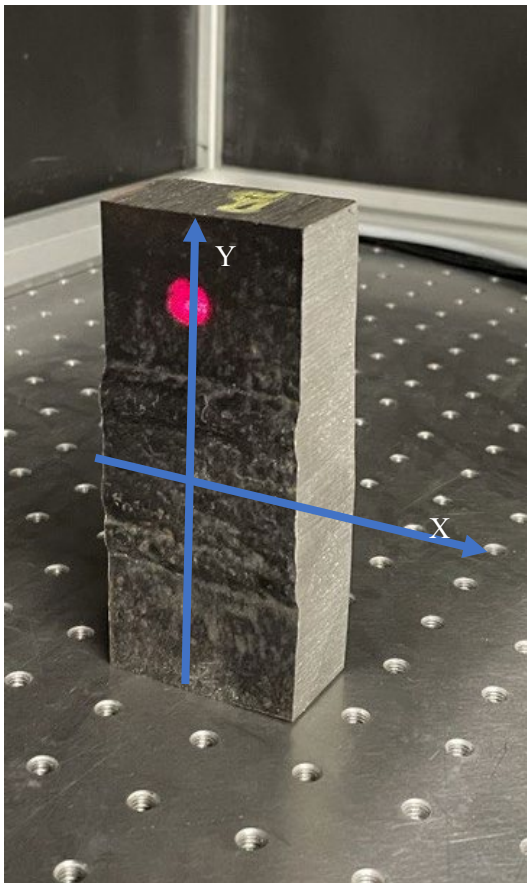

1Hz									
Base Metal	NO-RS	5x1.000ms	50%	12.5 fps	Base Metal	Y-RS	5x1.000ms	50%	12.5 fps
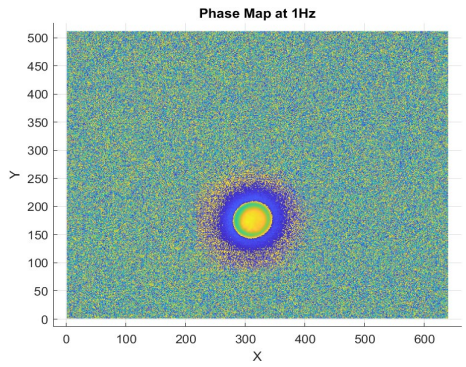					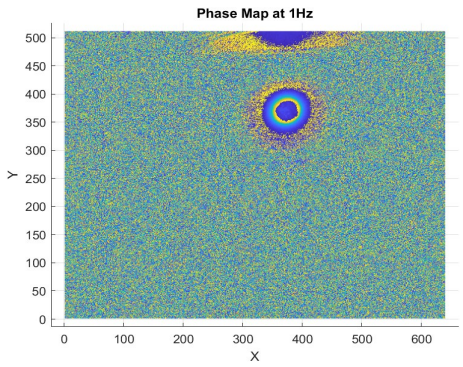				
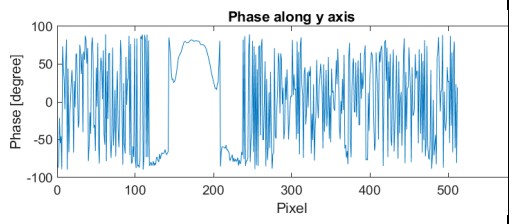					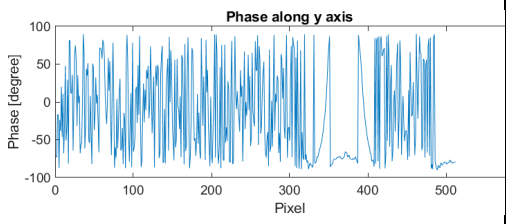				
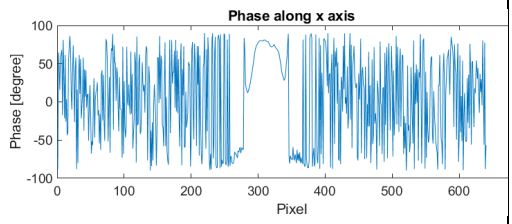					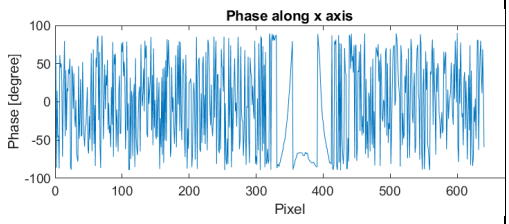				

0.1Hz									
Base Metal	NO_RS	5x10.000ms	25%	3 fps		Base Metal	Y_RS	5x10.000ms	25%	3 fps
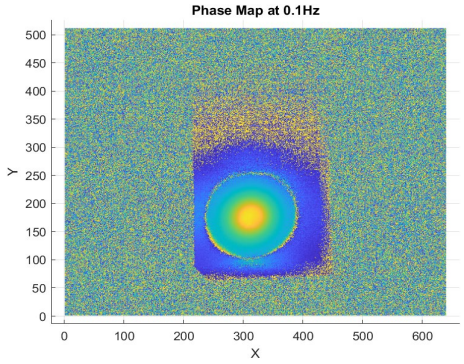						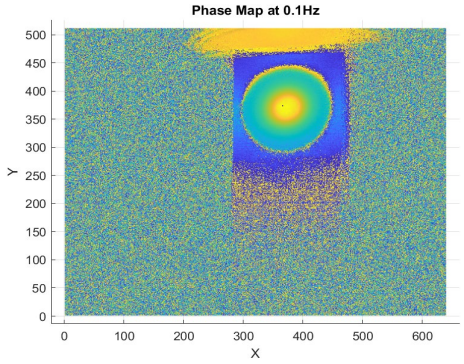				
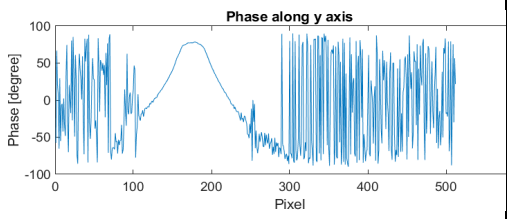						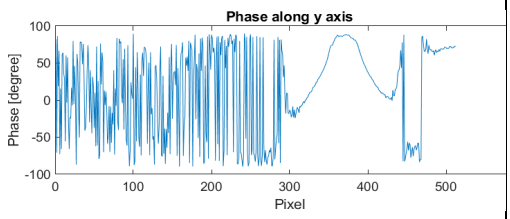				
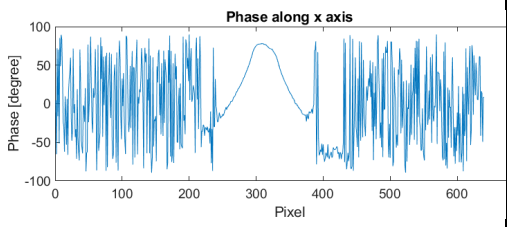						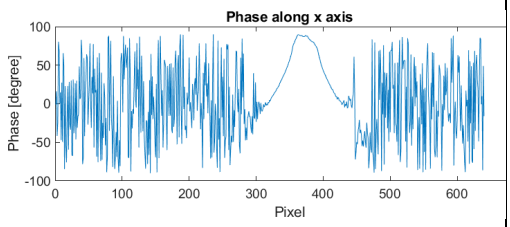				

1Hz									
Weld Bead	NO_RS	5x1.000ms	50%	12.5 fps	Weld Bead	Y_RS	5x1.000ms	50%	12.5 fps
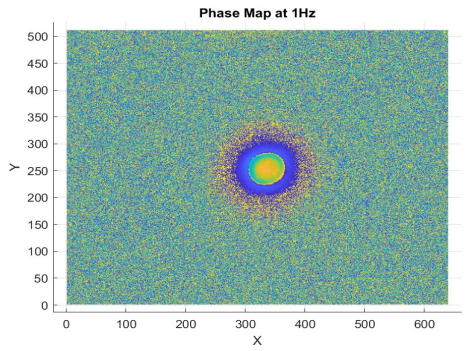					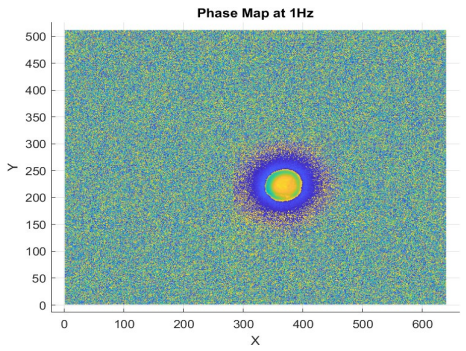				
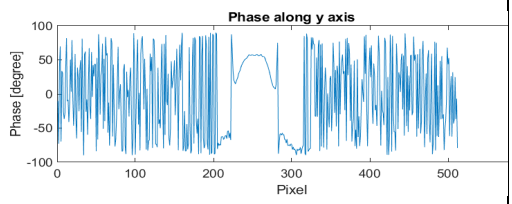					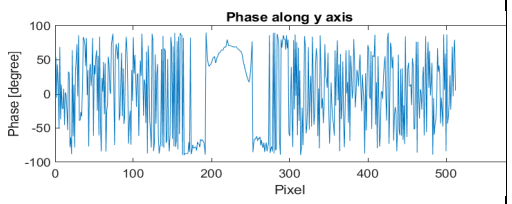				
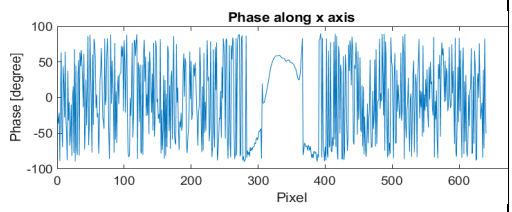					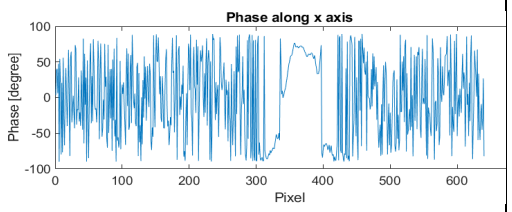				

0.1Hz									
Weld Bead	NO_RS	5x10.000ms	25%	3 fps		Weld Bead	Y_RS	5x10.000ms	25%	3 fps
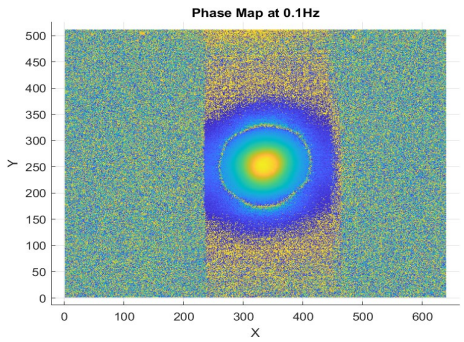						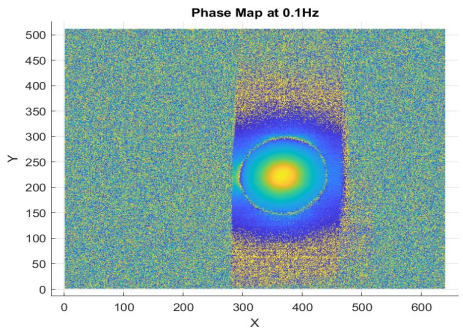				
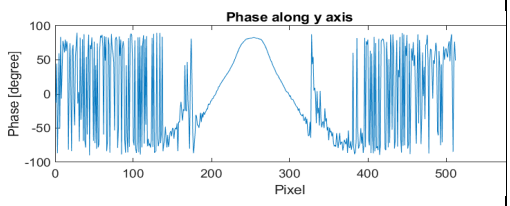						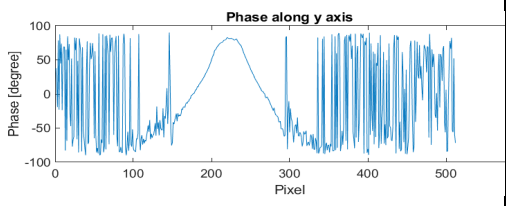				
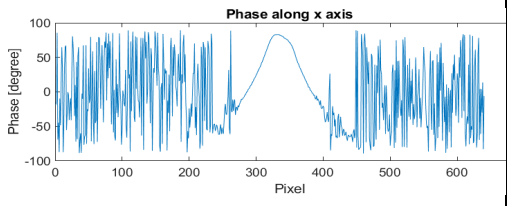						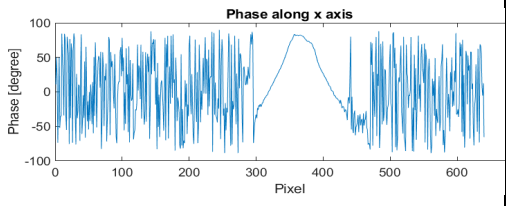				

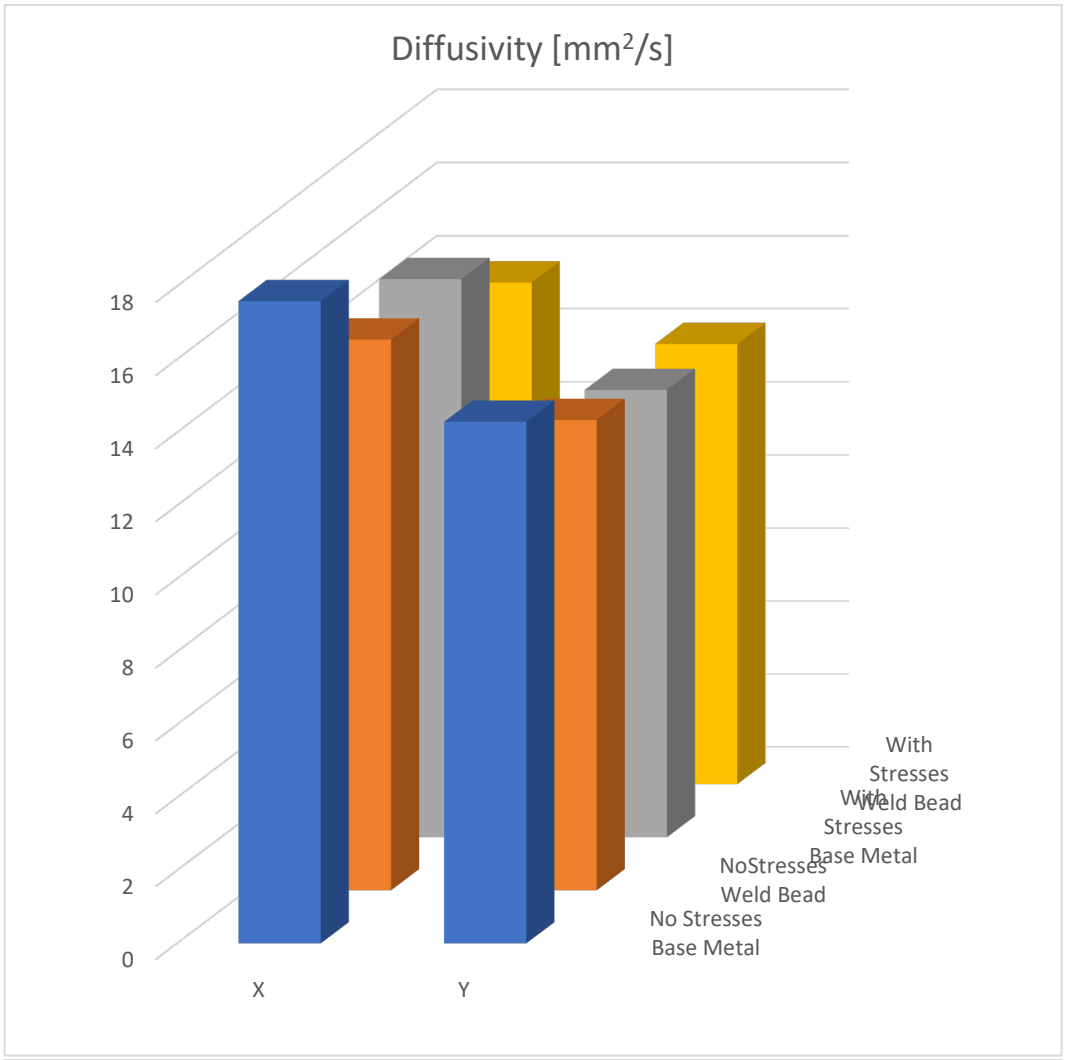
Diffusivity [mm²/s]
18
16
14
12
10
8
6
4
2
0
X
Y
No Stresses
Base Metal
NoStresses
Weld Bead
With
Stresses
Base Metal
With
Stresses
Weld Bead

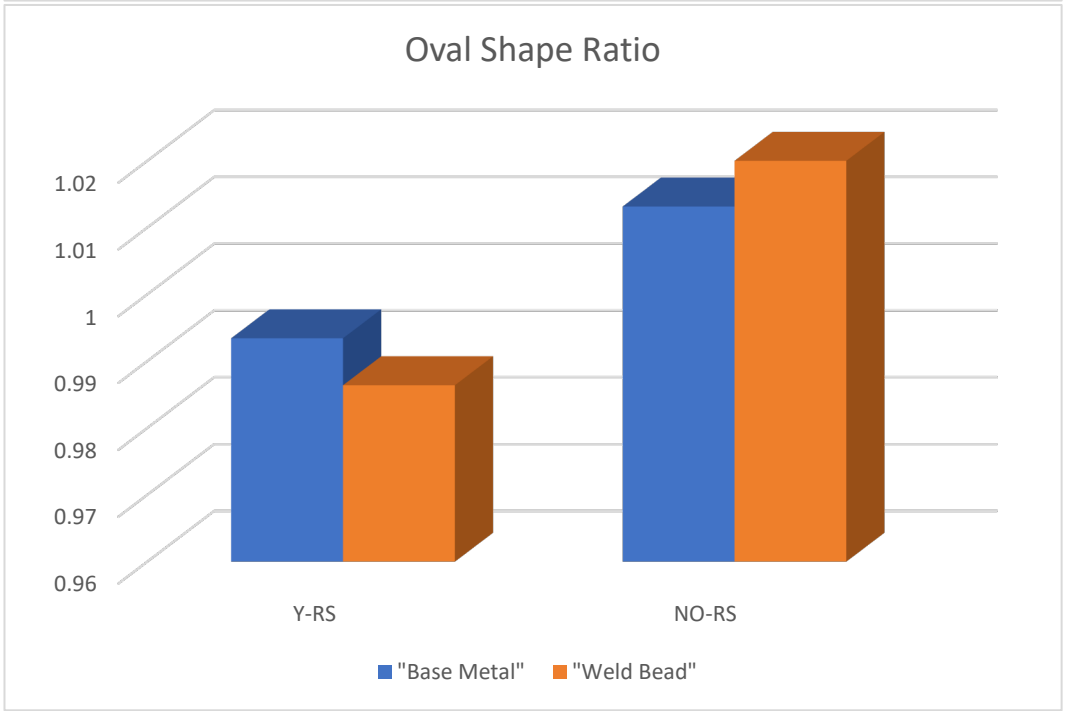
Oval Shape Ratio
1.02
1.01
1
0.99
0.98
0.97
0.96
Y-RS
NO-RS
"Base Metal"
"Weld Bead"

			Diffusivity	[mm²/s]	
		Zone	X	Y	X/Y %
1Hz	No RS	Base Metal	5.4	5.5	97.4
		Weld Bead	41.3	26.3	156.8
	with RS	Base Metal	6.6	5.7	115.4
		Weld Bead	23.9	29.0	82.34
0.1Hz	NoRS	Base Material	17.5	14.2	123.0
		Welding	15.0	12.8	117.0
	With RS	Base Material	15.2	12.2	124.7
		Welding	13.7	12.0	113.9

Comments

As regarding the diffusivity information extracted at 1Hz, is really difficult to have clean data because of the high sensitivity of the method of extraction of the diffusivity on the slope of the phase. The final values cannot be trust.

The diffusivity information extracted with a modulation frequency of the laser at 0.1Hz show a clear phase diagram and is also possible to easily pick the slope information from it. Here the diffusivity data are more reliable and can be seen how the X/Y ration between the tests on base material is the same 123% for both tests probably due to the inclination of the camera, while the ratio in the welding zone is different.

Even though the short number of impulse of the laser doesn't lead to a stabilization of the of the thermogram the result obtained with 0.1Hz modulation frequency of the laser are more reliable and clean. This make sense as discussed in [3]because lower frequencies avoid diffraction phenomena and are preferred when the slab is large enough to avoid boundary effects

The test performed on the top surface of the welding, which is highly irregular, has shown a better behaviour during low frequency/low power tests than in high frequency/ high power tests. Furthermore with improvement of signal processing algorithm lower and

lower power should be used to reach a lock-in test with an ideal peak temperature of less then 5K over the environmental temperature to avoid heat losses with air which leads to non-linearities.

No information can be extrapolated from oval aspect ratio, in fact the only correlation analytically demonstrated between thermograms and diffusivity is the one with the slope of the phase or temperature with their appropriate scale factor.[32], [33]

Metallographic analysis

The specimen have been named:

- 1 : Specimen without residual stresses
- 2 : Specimen with residual stresses

For each specimen has been analysed 3 section with 2 different zoom , 5x and 50x:

- Base Metal
- HAZ
- Weld bead

The smoothing has been ended at 1 μm and the chemical etching has been done with NITAL 4%.

Comments

The base metal is a C30. The microstructure shows geometries characteristic of the lamination process. In particular it is possible to see the dark and elongated grains of fine perlite in a matrix of equiaxed grains of ferrite.

The two welds, on the other hand, have profound differences, as far as the weld bead of the specimen 1 is concerned, a lower bainitic structure is noted, while for the specimen 2 the weld has a martensitic structure with probable residual austenite that cannot be resolved at this magnification.

In the heat affected zone, the main phenomenon is a generalized diffusion of the cementite towards the grain boundaries.

Specimen 1

Base metal

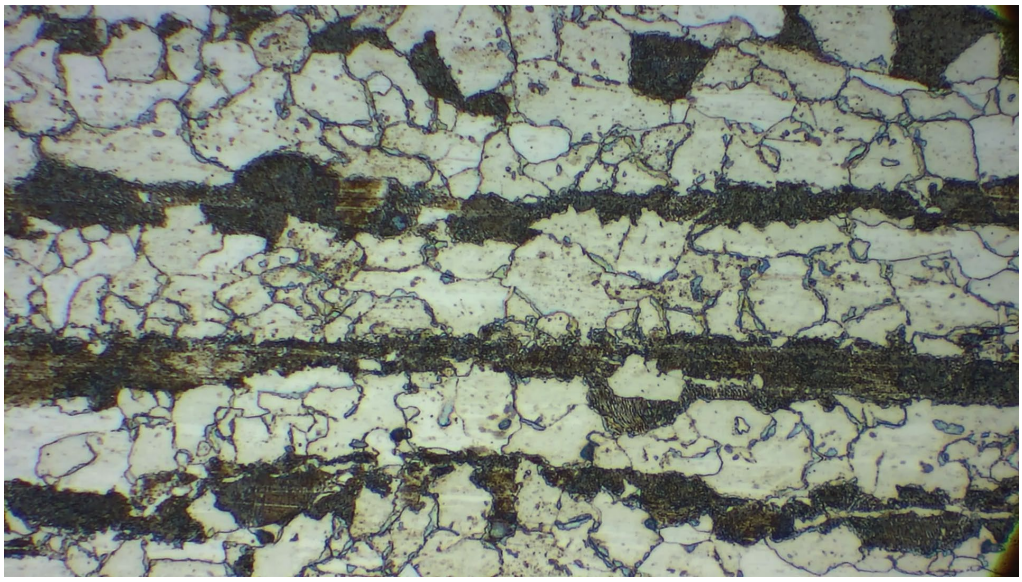

Figure 1 Base Metal 50x

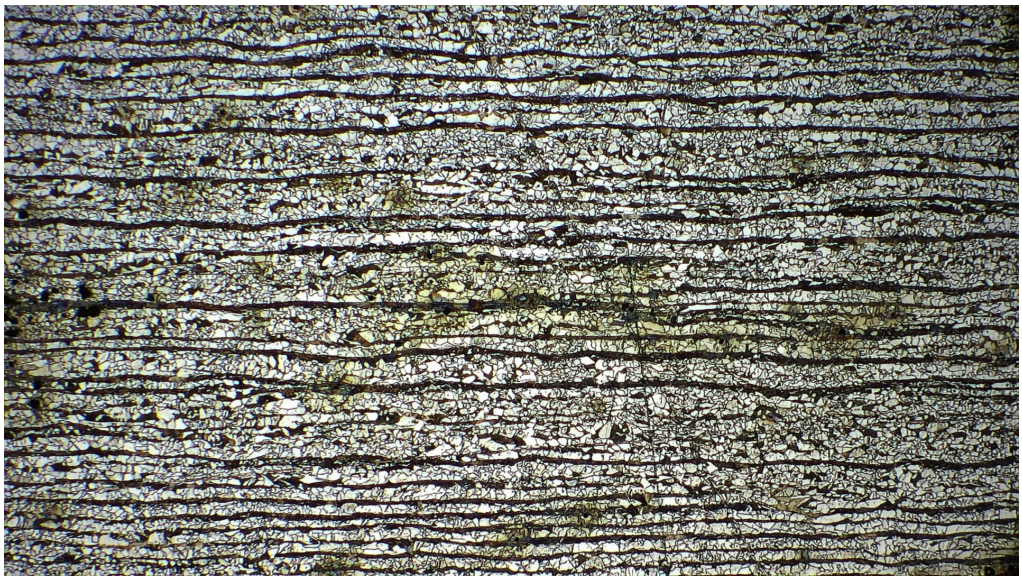

Figure 2 Base Metal 5x

HAZ

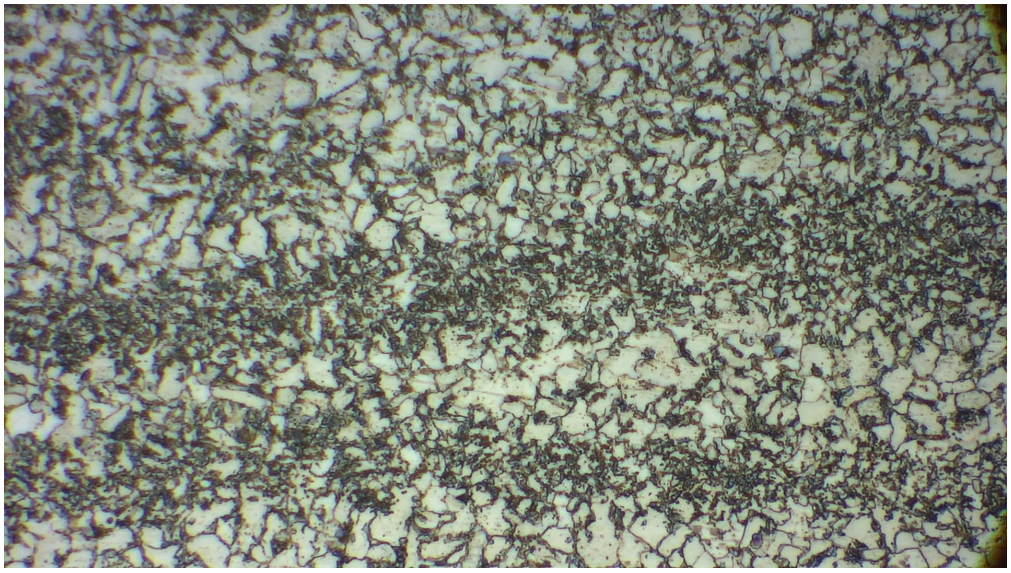

Figure 3 HAZ 50x

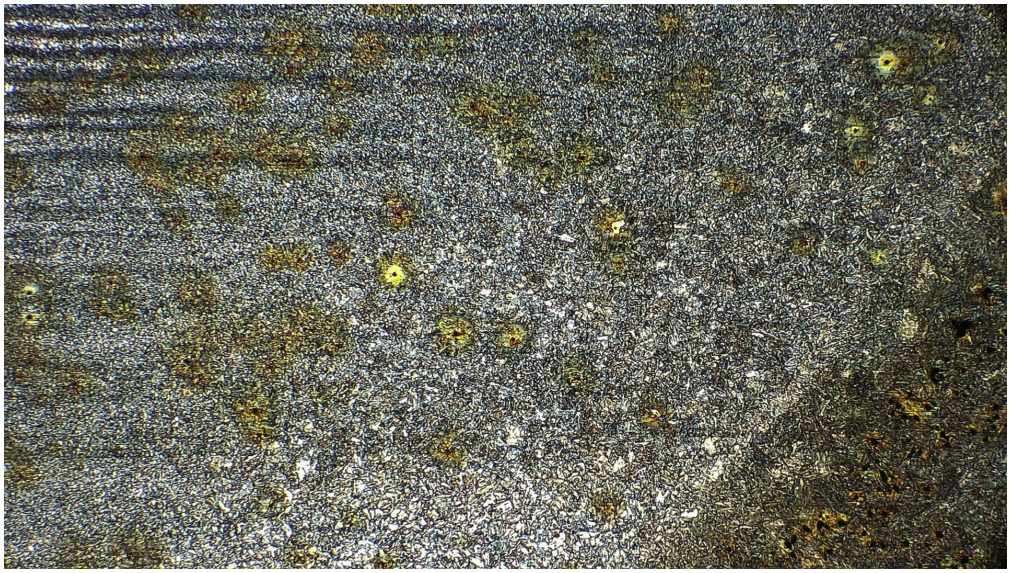

Figure 4 HAZ 5x

Weld bead

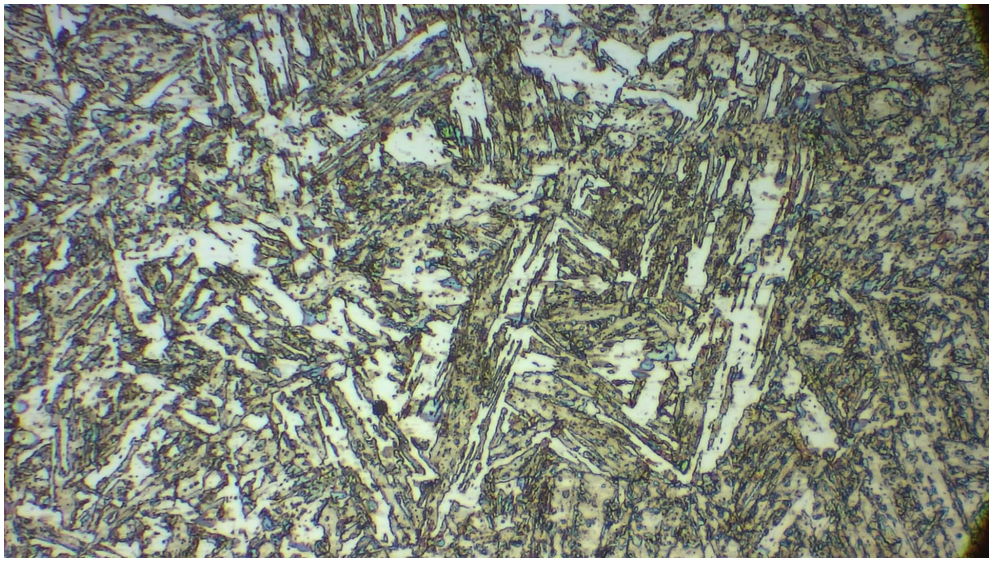

Figure 5 Weld Bead 50x

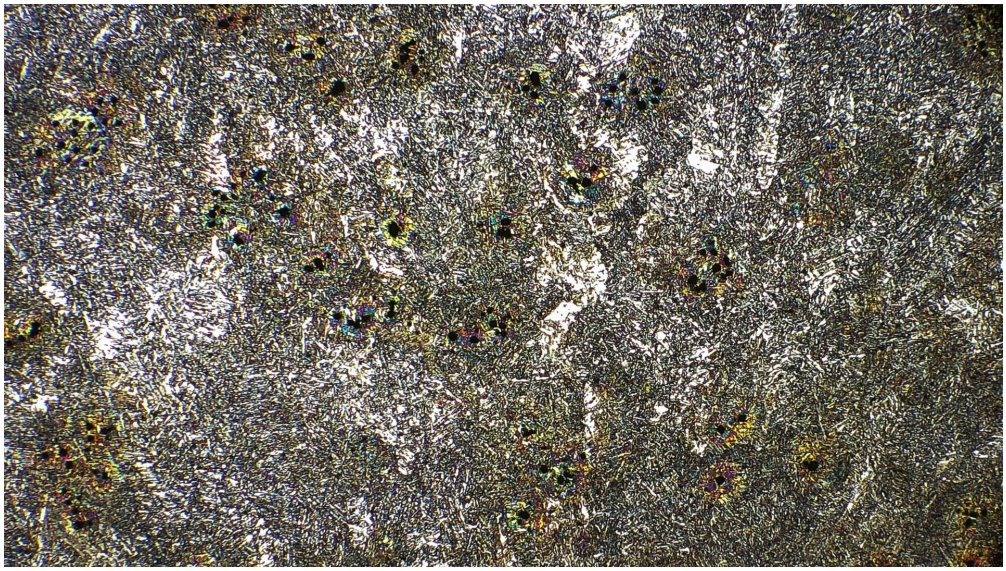

Figure 6 Weld Bead 5x

Specimen 2

Base metal

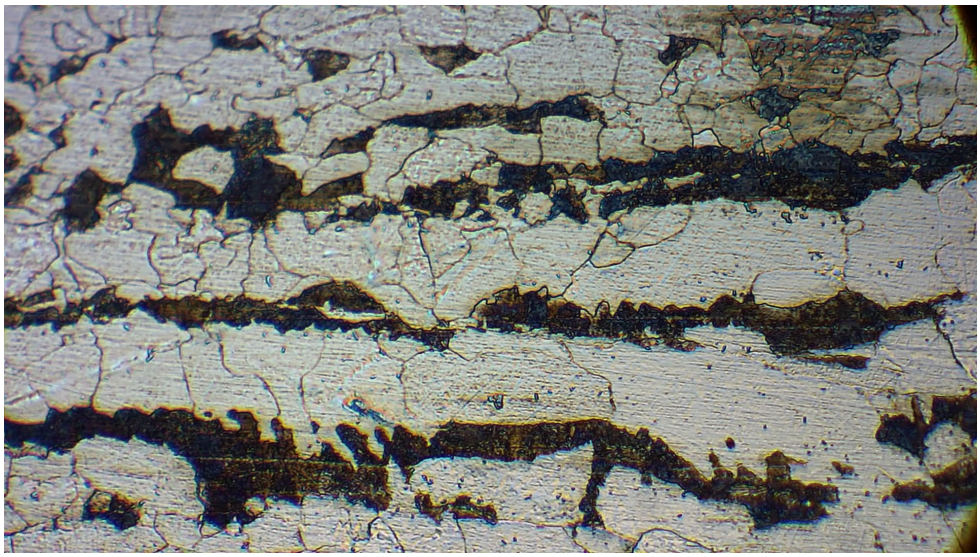

Figure 7 Base Metal 50x

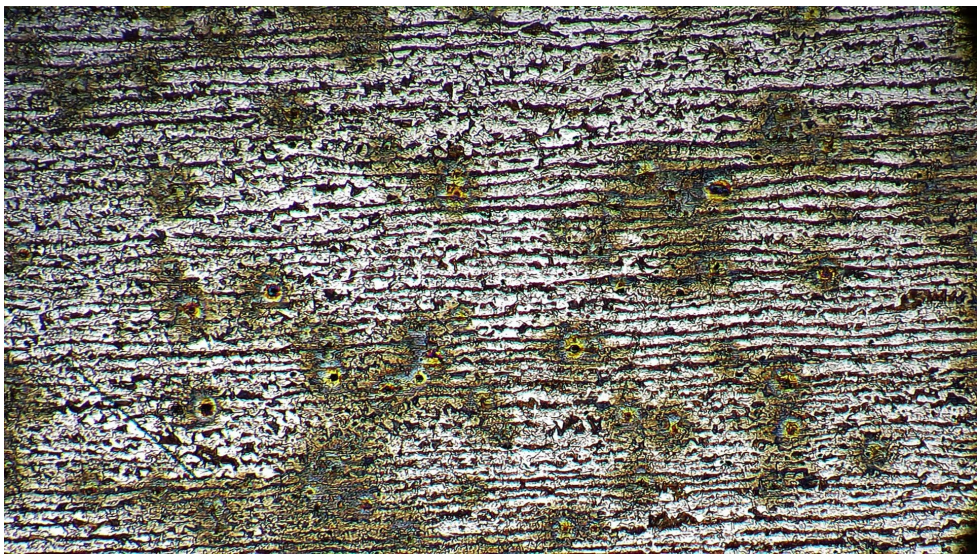

Figure 8 Base Metal 5x

HAZ

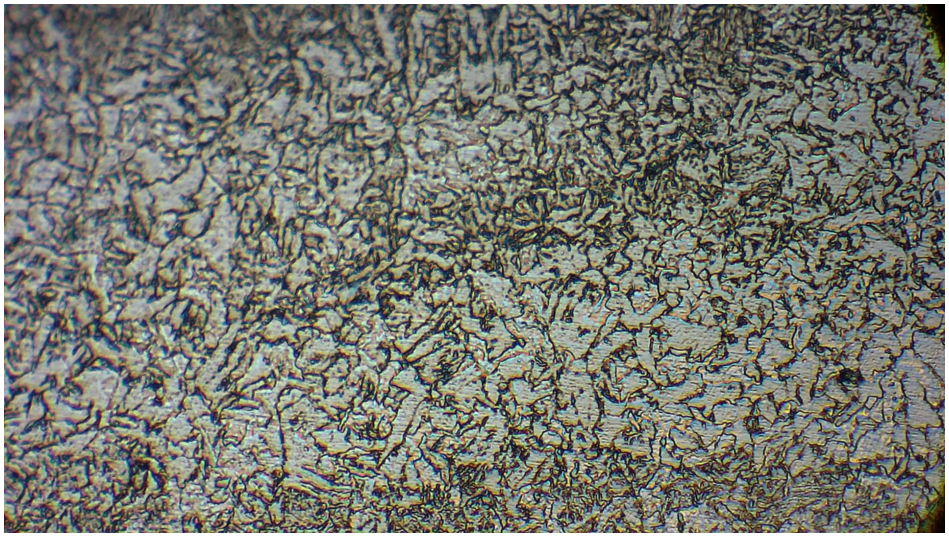

Figure 9 HAZ 50x

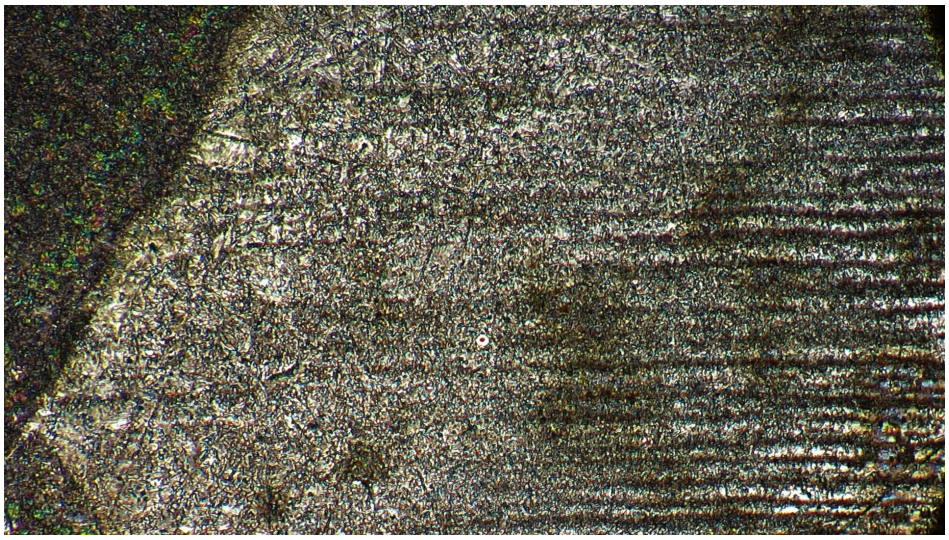

Figure 10 HAZ 5x

Weld bead

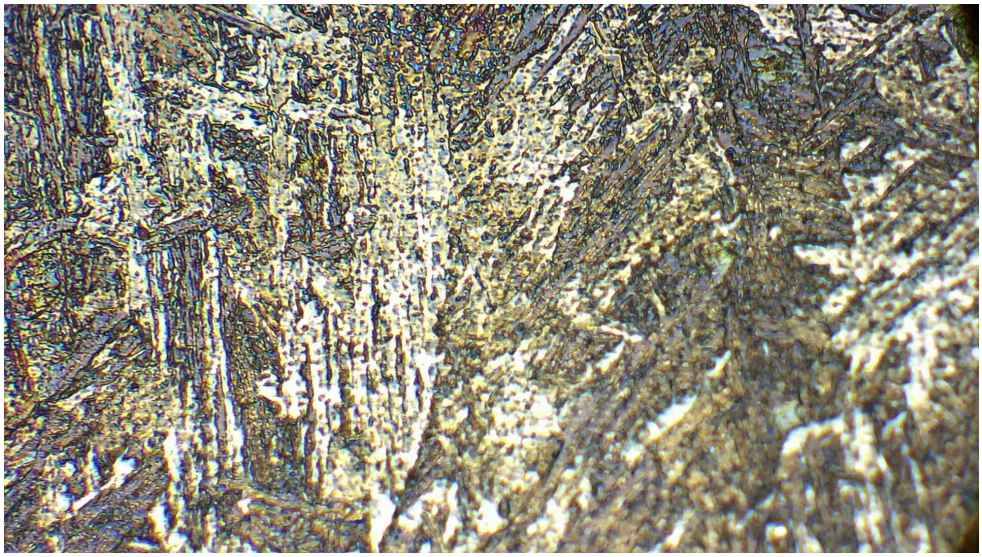

Figure 11 Weld Bead 50x

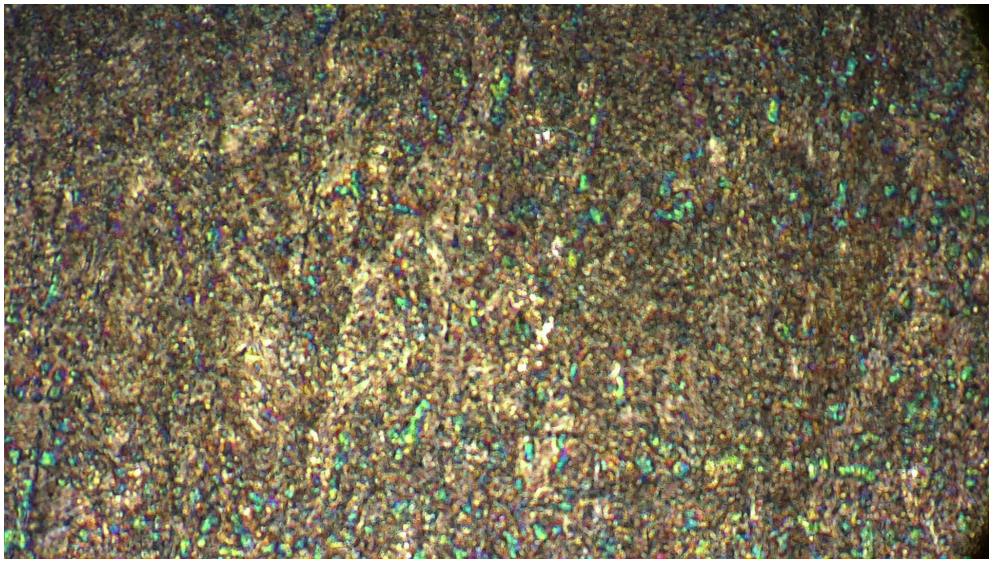

Figure 12 Weld Bead 5x

Conclusions

The laser spot lock-in thermography has great potential, however needs a great calibration effort in comparison with the lamp lock-in thermography.

This work is a first approach to the investigation of residual stresses in weldings, one of the main issue is related to the presence of different microstructures in the different parts of the specimen.

Another issue is the difficulty to obtain same test condition between different tests set-up when we use short impulses, it means that as far as we move the position of the laser in the surface the results changes. This is one of the main reason because we choose the lock-in thermography instead of pulsed. In fact, having only a qualitative comparison using pulsed-IRT is not reliable. The pulsed thermography is sensitive to the local photo-thermal parameter and this, in the case of a 'real' welded specimen which doesn't reach an high homogeneity on the surface, makes the method non reliable.

At the same time I have to say that the same problem related to photo-thermal inhomogeneities on the surface creates problem in the amplitude map from lock-in tests. This the reason why, for the first approach, the phase map has been chosen to calibrate the parameters. In addition the phase method is commonly used in literature and this makes possible to have a better background to perform a good setup of the equipment (laser head, thermal camera, signal processing algorithm). By first guess we decided to use low laser modulation frequencies, as suggested in literature, between 1Hz and 0.1Hz.

The main parts of the work has focused on calibration of the test parameter and signal processing algorithm. One of the main problem has been the computational time, this is why different methods are proposed. Some tests have been done on the different kind of results representation, as said before, and we decide to exclude for this first approach to residual stresses investigation the pulsed thermography and the amplitude map at lock-in frequency. We even tried to uncouple the pulsed thermogram by the boundary condition trying to process the thermal decay shape to extract some characteristic parameters but this isn't possible and reliable.

Then we compared the effect of temperature rises during lock in thermography using as constrain parameter the laser's power instead of the absolute maximum temperature rises so we were able to characterize the test by the heat input and to see the diffusion of the heat into the bulk of the material. The reason of this choice can be linked to the same consideration as before, that is the need to uncouple the test parameter setup from the

surface characteristics trying to see into the bulk of the material. However by the thermogram's recording we see only the surface, and not the bulk of the material, so is better to don't use that information as constrains in the choice of the laser power output level. So, the comparison has been done between 11% and 40% laser's power level , obviously the tests performed with a 40% laser's power level have reached higher temperature's peak. The results of this tests show that with higher temperature peak we have more difficult to read the phase map because more non-linearities are induced by heat losses with the air and high gradient plots.

Starting from the precedent results it was possible to understand that we need to set the parameter in order to achieve a smoother diffusion of the heat in the material. So the other tests investigated the improve in the quality of the results using a 0.1Hz and 1Hz frequency and halving the power level in the lower frequency test. Here the most interesting results were achieved. The 0.1Hz laser's modulation frequency tests permits us to reach a really good quality of the phase map plot. As far as we care about the thermogram we continued to have noised zones but the 'phase cut' plots show a really smooth transition between the zone of the laser spot and the sloping zone of diffusion along the surface . This make easy to measure the slope and to elaborate it to quantify the thermal diffusivity.

In the end we can say that the thermal diffusivity increases along the direction orthogonal to the weld bead in the case of residual stresses. However more test are required to reach a good accuracy for different kind of welding specs.

This is an innovative technique never used for this kind of investigation, in addition is one of the few non destructive testing method which can be performed on weldings.

References

[1] S. Doshvarpassand, C. Wu, and X. Wang, “An overview of corrosion defect characterization using active infrared thermography,” *Infrared Physics and Technology*, vol. 96. Elsevier B.V., pp. 366–389, Jan. 01, 2019. doi: 10.1016/j.infrared.2018.12.006.

[2] S. Paoloni, M. E. Tata, F. Scudieri, F. Mercuri, M. Marinelli, and U. Zammit, “IR thermography characterization of residual stress in plastically deformed metallic components,” *Applied Physics A: Materials Science and Processing*, vol. 98, no. 2, pp. 461–465, Feb. 2010, doi: 10.1007/s00339-009-5422-9.

[3] A. Mendioroz, R. Fuente-Dacal, E. Apianiz, and A. Salazar, “Thermal diffusivity measurements of thin plates and filaments using lock-in thermography,” *Review of Scientific Instruments*, vol. 80, no. 7, 2009, doi: 10.1063/1.3176467.

[4] B. P. Epps and E. M. Krivitzky, “Singular value decomposition of noisy data: noise filtering,” *Experiments in Fluids*, vol. 60, no. 8, Aug. 2019, doi: 10.1007/s00348-019-2768-4.

[5] B. P. Epps and E. M. Krivitzky, “Singular value decomposition of noisy data: mode corruption,” *Experiments in Fluids*, vol. 60, no. 8, Aug. 2019, doi: 10.1007/s00348-019-2761-y.

[6] B. P. Epps and A. H. Techet, “An error threshold criterion for singular value decomposition modes extracted from PIV data,” *Experiments in Fluids*, vol. 48, no. 2, pp. 355–367, Feb. 2010, doi: 10.1007/s00348-009-0740-4.

[7] Tzou Da You, “Thermal shock phenomena under high rate response in solids chapter three (111-185)”.

[8] D. Y. Tzou and Z. Y. Guo, “Nonlocal behavior in thermal lagging,” *International Journal of Thermal Sciences*, vol. 49, no. 7, pp. 1133–1137, Jul. 2010, doi: 10.1016/j.ijthermalsci.2010.01.022.

[9] Z. Y. Guo and Q. W. Hou, “Thermal wave based on the thermomass model,” *Journal of Heat Transfer*, vol. 132, no. 7, pp. 1–6, Jul. 2010, doi: 10.1115/1.4000987.

[10] Z. Y. Guo and Q. W. Hou, “Thermal wave based on the thermomass model,” *Journal of Heat Transfer*, vol. 132, no. 7, pp. 1–6, Jul. 2010, doi: 10.1115/1.4000987.

[11] M. Zheng, Z. Yuan, Q. Tong, G. Zhang, and W. Zhu, “A novel unconditionally stable explicit integration method for finite element method,” *Visual Computer*, vol. 34, no. 5, pp. 721–733, May 2018, doi: 10.1007/s00371-017-1410-9.

[12] H. P. Langtangen and S. Linge, “Finite difference methods for wave equations,” 2016.

[13] A. Quarteroni, F. Saleri, and P. Gervasio, *Calcolo Scientifico*, vol. 105. Milano: Springer Milan, 2017. doi: 10.1007/978-88-470-3953-7.

[14] X. Ai and B. Q. Li, “Numerical Simulation of Thermal Wave Propagation during Laser Processing of Thin Films,” 2005.

[15] C. Canuto, “Notes on Partial Differential Equations (Theory),” 2009. [Online]. Available: http://calvino.polito.it/∼ccanuto

[16] W. Wu and X. Li, “Application of the time discontinuous Galerkin finite element method to heat wave simulation,” *International Journal of Heat and Mass Transfer*, vol. 49, no. 9–10, pp. 1679–1684, May 2006, doi: 10.1016/j.ijheatmasstransfer.2005.10.025.

[17] F. Wang and E. Hou, “A Direct Meshless Method for Solving Two-Dimensional Second-Order Hyperbolic Telegraph Equations,” *Journal of Mathematics*, vol. 2020, 2020, doi: 10.1155/2020/8832197.

[18] R. Jiwari, S. Pandit, and R. C. Mittal, “A differential quadrature algorithm to solve the two dimensional linear hyperbolic telegraph equation with Dirichlet and Neumann boundary conditions,” *Applied Mathematics and Computation*, vol. 218, no. 13, pp. 7279–7294, Mar. 2012, doi: 10.1016/j.amc.2012.01.006.

[19] “The Finite Element Method: Its Basis and Fundamentals.”

[20] Z. Ming, G. Qintao, Y. Lin, and Z. Baoqiang, “Finite element model updating of jointed structure based on modal and strain frequency response function,” *Journal of Mechanical Science and Technology*, vol. 33, no. 10, pp. 4583–4593, Oct. 2019, doi: 10.1007/s12206-019-0902-0.

[21] Z. B. Yang, Z. K. Wang, S. H. Tian, and X. F. Chen, “Analysis and modelling of non-fourier heat behavior using the wavelet finite element method,” *Materials*, vol. 12, no. 8, 2019, doi: 10.3390/ma12081337.

[22] M. Torabi and K. Zhang, “Multi-dimensional dual-phase-lag heat conduction in cylindrical coordinates: Analytical and numerical solutions,” *International Journal of Heat and Mass Transfer*, vol. 78, pp. 960–966, 2014, doi: 10.1016/j.ijheatmasstransfer.2014.07.038.

[23] B. Yu, X. Jiang, and C. Wang, “Numerical algorithms to estimate relaxation parameters and Caputo fractional derivative for a fractional thermal wave model in spherical composite medium,” *Applied Mathematics and Computation*, vol. 274, pp. 106–118, Feb. 2016, doi: 10.1016/j.amc.2015.10.081.

[24] F. Nasri, M. F. ben Aissa, and H. Belmabrouk, “Microscale thermal conduction based on Cattaneo-Vernotte model in silicon on insulator and Double Gate MOSFETs,” *Applied Thermal Engineering*, vol. 76, pp. 206–211, Feb. 2015, doi: 10.1016/j.applthermaleng.2014.11.038.

[25] N. Torabian, V. Favier, S. Ziaei-Rad, J. Dirrenberger, F. Adamski, and N. Ranc, “Thermal response of DP600 dual-phase steel under ultrasonic fatigue loading,” *Materials Science and Engineering A*, vol. 677, pp. 97–105, Nov. 2016, doi: 10.1016/j.msea.2016.09.025.

[26] Y. Wang, G. Y. Tian, and B. Gao, “Eddy Current and Thermal Propagation for Quantitative NDT&E,” 2016. [Online]. Available: http://creativecommons.org/licenses/by/3.0/

[27] E. Thiel, M. Kreutzbruck, and M. Ziegler, “Laser Projected Photothermal Thermography for Characterizing Hidden Defects,” 2016.

[28] F. Lopez, X. Maldague, C. Ibarra, and − Castanedo, “Enhanced image processing for infrared non-destructive testing,” 2014, doi: 10.2478/s11772−014−0202−2.

[29] J. Roemer, Ł. Pieczonka, U. Agh, A. Górniczo-Hutnicza, K. Robotyki, and M. A. Al, “LASER SPOT THERMOGRAPHY OF WELDED JOINTS,” 2014.

[30] M. Honner, P. Litoš, and M. Švantner, “Thermography analyses of the hole-drilling residual stress measuring technique,” *Infrared Physics and Technology*, vol. 45, no. 2, pp. 131–142, Mar. 2004, doi: 10.1016/j.infrared.2003.08.001.

[31] H. Vemanaboina, G. Edison, and S. Akella, “Weld bead temperature and residual stresses evaluations in multipass dissimilar INCONEL625 and SS316L by GTAW using IR thermography and x-ray diffraction techniques,” *Materials Research Express*, vol. 6, no. 9, Jul. 2019, doi: 10.1088/2053-1591/ab3298.

[32] N. Rajic and C. Antolis, “An investigation of noise performance in optical lock-in thermography,” *Infrared Physics and Technology*, vol. 87, pp. 1–10, Dec. 2017, doi: 10.1016/j.infrared.2017.09.019.

[33] C. Maierhofer, P. Myrach, R. Krankenhagen, M. Röllig, and H. Steinfurth, “Detection and characterization of defects in isotropic and anisotropic structures using lockin thermography,” *Journal of Imaging*, vol. 1, no. 1, pp. 220–248, Dec. 2015, doi: 10.3390/jimaging1010220.

[34] O. (Otwin) Breitenstein, W. (Wilhelm) Warta, and M. (Martin) Langenkamp, *Lock-in thermography : basics and use for evaluating electronic devices and materials*. Springer, 2010.